

On the Interplay between Distributed Bulk Plasticity and Local Fault Slip in Evolving Fault Zone Complexity

Mohamed Abdelmeguid¹, Md Shumon Mia², and Ahmed Elbanna³

¹California Institute of Technology

²University of Illinois at Urbana-Champaign

³University of Illinois Urbana

January 15, 2024

Abstract

We numerically investigate the role of plastic strain accumulation on the mechanical response of a planar strike-slip fault. Our models show that fault-zone strength significantly impact the ensuing sequence of earthquakes. Weaker fault zones accumulating more plastic strain promote more complexity in the seismicity pattern through aperiodic earthquake occurrences and intermittent episodes of rupture and arrest. However, if the fault zone strength is high enough, the overall earthquake sequence is characterized by periodic fault-spanning events. We find that both the fault normal stress and the fault surface profile evolve throughout the earthquake sequence, suggesting a self-roughening mechanism. Despite the significant impact of plasticity on the fault response, the width of the plastically deforming region in the fault zone is small compared to the fault length. Our results suggest a rich behavior in dynamically evolving fault zones and support the need for further high-resolution studies of the highly non-linear near-fault region.

On the Interplay between Distributed Bulk Plasticity and Local Fault Slip in Evolving Fault Zone Complexity

Mohamed Abdelmeguid^a, Md Shumon Mia^{b,c}, and Ahmed Elbanna^{b,d}

^aGraduate Aerospace Laboratories, California Institute of Technology, Pasadena, CA, USA.

^bDepartment of Civil and Environmental Engineering, University of Illinois at Urbana-Champaign, Urbana, IL, USA

^cDepartment of Mechanical Science and Engineering, University of Illinois at Urbana-Champaign, Urbana, IL, USA

^dBeckman Institute of Advanced Science and Technology, University of Illinois at Urbana-Champaign, Urbana, IL, USA,

*e-mail: meguid@caltech.edu

Key Points:

- Partitioning of deformation between bulk and fault contribute to seismic complexity.
- Seismic complexity and accumulation of plastic strain induce normal stress perturbations on the fault.
- Off-fault inelastic deformation result in cascading earthquake.

Abstract

We numerically investigate the role of plastic strain accumulation on the mechanical response of a planar strike-slip fault. Our models show that fault-zone strength significantly impact the ensuing sequence of earthquakes. Weaker fault zones accumulating more plastic strain promote more complexity in the seismicity pattern through aperiodic earthquake occurrences and intermittent episodes of rupture and arrest. However, if the fault zone strength is high enough, the overall earthquake sequence is characterized by periodic fault-spanning events. We find that both the fault normal stress and the fault surface profile evolve throughout the earthquake sequence, suggesting a self-roughening mechanism. Despite the significant impact of plasticity on the fault response, the width of the plastically deforming region in the fault zone is small compared to the fault length. Our results suggest a rich behavior in dynamically evolving fault zones and support the need for further high-resolution studies of the highly non-linear near-fault region.

Plain Language Summary

Why do some faults fail in large earthquakes while other faults generate smaller ones? In our computer simulation study, we explored how the strength of a strike-slip fault (where Earth's crust plates slide past each other) affects earthquake patterns. We discovered that weaker fault zones, which can stretch or squeeze more, often have more complex and unpredictable earthquake patterns, including irregular timings and smaller, clustered earthquakes. In contrast, stronger fault zones tend to have regular, larger earthquakes. Interestingly, in weaker fault zones, the geometry of the fault surface can change over time and become rougher in response to the

39 deformability of the surrounding rocks, suggesting a roughening of the fault surface. Although
40 these changes significantly influence earthquake patterns, they occur in a relatively small region
41 surrounding fault surfaces highlighting the need for expanding instrumentation closer to active
42 faults. These findings are useful for contextualizing observed seismicity patterns and are relevant
43 for seismic hazard studies.

44 1 Introduction

45 Geological observations of fault zones highlight a region of pervasive damage that surrounds
46 the principal slip surfaces [1–7]. A typical strike slip fault zone may have one or more fault
47 cores with damage features at varying length scales from fine scale distributed damage to more
48 discrete anisotropic secondary faults. In general, the distribution and intensity of damage decays
49 away from the main fault, leading to a gradual transition from a damaged zone to intact host
50 rock [2, 8]. Extensive studies on damaged fault zones reveal substantial differences between
51 the mechanical properties of the inner fault zone core compared to the host rock material [9,
52 10]. This variation in fault zone properties was found to influence many rupture characteristics
53 including rupture directivity [11], rupture speed, high frequency generation [12], maximum
54 event magnitude [13], radiation patterns [14–18] and surface deformation [19].

55 Fault zone damage may accumulate both seismically and aseismically [1, 2, 20, 21] and is
56 generally enhanced in the presence of geometrical complexity [22–30]. Prior studies suggest that
57 regardless of the damage generation mechanism, the scale of damage evolution varies based on
58 the maturity of the fault core [31]. Specifically, fault zone damage scales with fault slip up a
59 certain threshold above which the fault zone width growth is minimal [8, 32]. Furthermore, the
60 damage density decreases exponentially or as a power law with distance normal to the fault
61 surface [8, 26, 33].

62 Fault zone damage has been studied extensively using dynamic rupture simulations [34–36]
63 using different idealizations including plasticity theories and continuum damage mechanics as
64 well as the limiting case of an elastic low velocity fault zone. Among the major conclusions
65 of these studies are that the damage region contributes to a heterogeneous local stress field on
66 the fault, acts as an energy sink increasing the total energy dissipated during dynamic rupture,
67 and leads to generation of trapped waves that may enhance high frequency generation and
68 influence the rupture mode. While, dynamic rupture simulations provide significant insight
69 into the accumulation and effects of damage during earthquake rupture. Field observation
70 indicates that damage accumulation on larger faults is associated with overprinting from multiple
71 slip events rather than a single dynamic event. To this point, earthquake cycle simulations
72 that are capable of modeling sequences of earthquakes are a prime candidate for the study of
73 evolving damage profiles on a fault zone. However, due to the numerical complexity of modeling
74 multiple earthquakes over different spatial and temporal scales, only a handful of earthquake
75 cycle studies investigated the effect of the bulk material response, beyond elasticity [21, 30,
76 37–39]. In anti-plane approximation, [38] utilized a combined finite element spectral boundary
77 integral scheme (FEBE) to investigate the effects of the bulk yield strength on the overall
78 sequence of the earthquake and aseismic slip and the evolution of inelastic strain. In that study,
79 they demonstrated that the partitioning between off-fault deformations and fault slip could lead
80 to a complex sequence of seismicity. However, within that study, the role of pressure-dependent
81 rock strength was neglected. Recently, Abdelmeguid and Elbanna demonstrated, in the context
82 of 2D plane-strain approximation, that there is a feedback mechanism between the evolution
83 of plastic strain in the bulk and mean stress which in turn influences the pressure-dependent
84 yield strength and subsequent generation of plastic strain [21]. Accordingly, it still remains to
85 be investigated whether the spatio-temporal clustering observed in the anti-plane model would
86 persist in the context of in-plane deformations, and what role the feedback between mean stress
87 and inelastic strain accumulation plays in fault zone maturity.

88 In this paper, we focus on aspects related to the co-evolution of seismicity and off-fault
89 viscoplastic bulk rheology. We consider the 2D plane-strain approximation as a minimal model
90 that enables us to study the role of pressure-dependent plasticity. We use a hybrid finite element
91 spectral boundary integral framework, FEBE, which accounts for the full inertia effect during
92 the seismic phase and enables accurate near field truncation of the wave field. We study the
93 evolution of the sequence of earthquakes and aseismic slip for different choices of bulk strength
94 and implications for event size distribution, partitioning of deformation, stress heterogeneity,
95 and fault surface evolution. We outline the setup of the model and summarize the main results
96 in the next section

97 2 Model Description

98 We consider a planar horizontal fault, with a right-lateral sense of motion, the frictional be-
99 havior is governed by rate-and-state friction under a 2D plane strain approximation. The fault
100 is bisecting an unbounded elastic-visco-plastic domain with homogeneous elastic properties as
101 shown in Figure A1a. The fault consists of a central velocity weakening patch surrounded by two
102 velocity strengthening patches and is being loaded from both ends by a constant plate loading
103 rate as shown in Figure A1b. The initial prestress σ_{ij}^0 shown in Figure A1b is assumed to be
104 uniform.

105 The bulk is initially assumed to be linear elastic. We use pressure-dependent Drucker-Prager
106 (DP) plasticity to describe the inelastic bulk response beyond the onset of yielding. The DP
107 yield surface is parameterized by two parameters: the angle of internal friction ϕ and cohesion
108 c . We assume a non-associative flow rule and Perzyna type viscous regularization. We vary the
109 value of the cohesion parameter c to explore the effect of fault zone strength on the evolution of
110 seismicity and near fault stresses and deformations. We implement normal stress regularization
111 on the fault surface following Prakash-Clifton law that ensures the fault local frictional strength
112 is a function of the history of the normal stress on the fault and eliminates any spurious unstable
113 modes that may emerge due to rapid variations in the instantaneous value of the normal stress
114 [40–42].

115 We use the FEBE framework presented in [21, 43] to explore the co-interplay between local-
116 ized fault slip and distributed bulk inelastic deformations through long sequences of earthquakes
117 and aseismic slip (SEAS). FEBE is a hybrid finite element spectral boundary integral scheme.
118 Spatially, FEBE adopts a domain decomposition approach where the near fault region that in-
119 cludes the potentially nonlinear material response is discretized using the finite element method.
120 The exterior half spaces beyond the near fault region are assumed to be linear elastic and ho-
121 mogeneous and are thus described by a spectral boundary integral formulation. The fault zone
122 and the exterior half spaces are coupled through the enforcement of continuity of traction and
123 displacement at their interfaces. The local nature of near-fault nonlinearities ensures that the
124 width of the discretized region W_s (shown in Figure A1b) is usually much smaller than the total
125 domain length L_T . The FEM domain size is selected such that the discretized domain contains
126 all the off-fault plasticity. For planar faults previous studies on dynamic fracture with off-fault
127 plasticity suggest that the extent of the plastic zone is proportional to the process zone size, this
128 estimate guides our initial choice of W_s [34, 44].

129 Temporally, FEBE implements an alternating quasi-dynamic scheme, to resolve interseismic
130 slow deformation while neglecting inertia effects, and a fully dynamic scheme, to resolve rapid
131 seismic periods while accounting for fully inertia effects. The switch between the two schemes is
132 determined by a velocity threshold. More details about the numerical algorithm may be found
133 in Abdelmeguid and Elbanna 2022 [21]. The values of the different parameters used in the model
134 are summarized in Table A1

3 Results

3.1 Spatial and Temporal Complexity

Figure 1a-d shows the temporal evolution, measured in simulation time steps, of the slip rate along the fault surface during the earthquake cycle for four different cases with decreasing cohesion. As discussed earlier, cohesion contributed to bulk strength. The lower the bulk cohesion, the more prone to yielding the fault zone becomes. We observe that as bulk strength decreases, spatio-temporal complexity of the earthquake sequence emerges. This is evident in the transition from periodic events with slight variation in the nucleation characteristics, at $c = 35$ MPa, to intermittent earthquake with strong rupture segmentation and temporal clustering, for $c = 22$ MPa. Similar to observations in the antiplane deformations [38] plasticity accumulation around the rupture tip may result in the pinning of the rupture which in turn leads to local rupture arrest and spatial segmentation of coseismic slip. For all four cases shown here, the pattern of seismicity varies. We show that based on the choice of cohesion the ensuing seismic cycle can include partial ruptures, slow events, and intermittent episodes of earthquakes. This complexity is a direct consequence of the competition between on-fault and off-fault deformations.

In the case of $c = 35$ MPa, most of the events within the sequence are periodic and through-going with shifts in the nucleation site. In the cases of $c = 30$ MPa, and $c = 26$ MPa the sequence of events are quasi-complex. For the case of $c = 30$ MPa, seismicity converges to a sequence of doublets: a partial rupture followed by a through-going rupture and this combination keeps repeating. For the case of $c = 26$ MPa, the spatio-temporal complexity increases. However, the complex pattern appears to approximately repeat itself over longer time scales. The end member case with $c = 22$ MPa shows no distinguishable pattern and no diminished complexity with time.

To demonstrate the temporal complexity induced by plastic strain accumulation in Figure 1e we compare the time history of the peak slip rate for the two cases of $c = 35$ MPa and $c = 22$ MPa. We observe significant differences between the two cases in terms of the inter-event time, peak slip rates, and the emergence of foreshocks and aftershocks. Figure 1f focuses on the seismic activity leading up to a number of mainshocks (marked by the stars) in the case of $c = 22$ MPa. Here, we define the mainshock as an event with peak slip rate exceeding 0.1 m/s. We observe that the slip rate on the fault surface doesn't change gradually, but rather through a burst of microseismicity leading up to the mainshock. This temporal complexity results from plasticity accumulation and stress redistribution which controls the growth and arrest of these transients. Zoomed-in panels in Figure 1f expand on this observation and by focusing on the few seconds to minutes around the time of occurrence of the main shock. What appears as a single spike in Figure 1e on the scale of years is indeed a complex sequence of clustered seismic activity with intermittent episodes of earthquakes characterized by closely spaced bursts of accelerated motion associated with spontaneous nucleation and arrest of the rupture front multiple times.

To further quantify the effect of plastic strain accumulation on seismicity pattern, we analyze the variability in some of the statistical characteristics of the seismic sequence with variations in the bulk strength. For example, Figure 1g-j shows the distribution of recurrence interval for each of the four values of the cohesion parameter investigated here. We observe that the choice of bulk strength has significant implications on the clustering of seismicity. At higher cohesion, the events are periodic in time with uniform interevent time (year). As the yield stress decrease, we observe a shift in the recurrence interval toward interevent times that are orders of magnitude smaller. Eventually, the recurrence interval distribution as shown in Figure 1j transitions to an almost bimodal distribution with a heavy tail that spans time scales from seconds to days. This transition is characteristic of the emergence of seismic swarms.

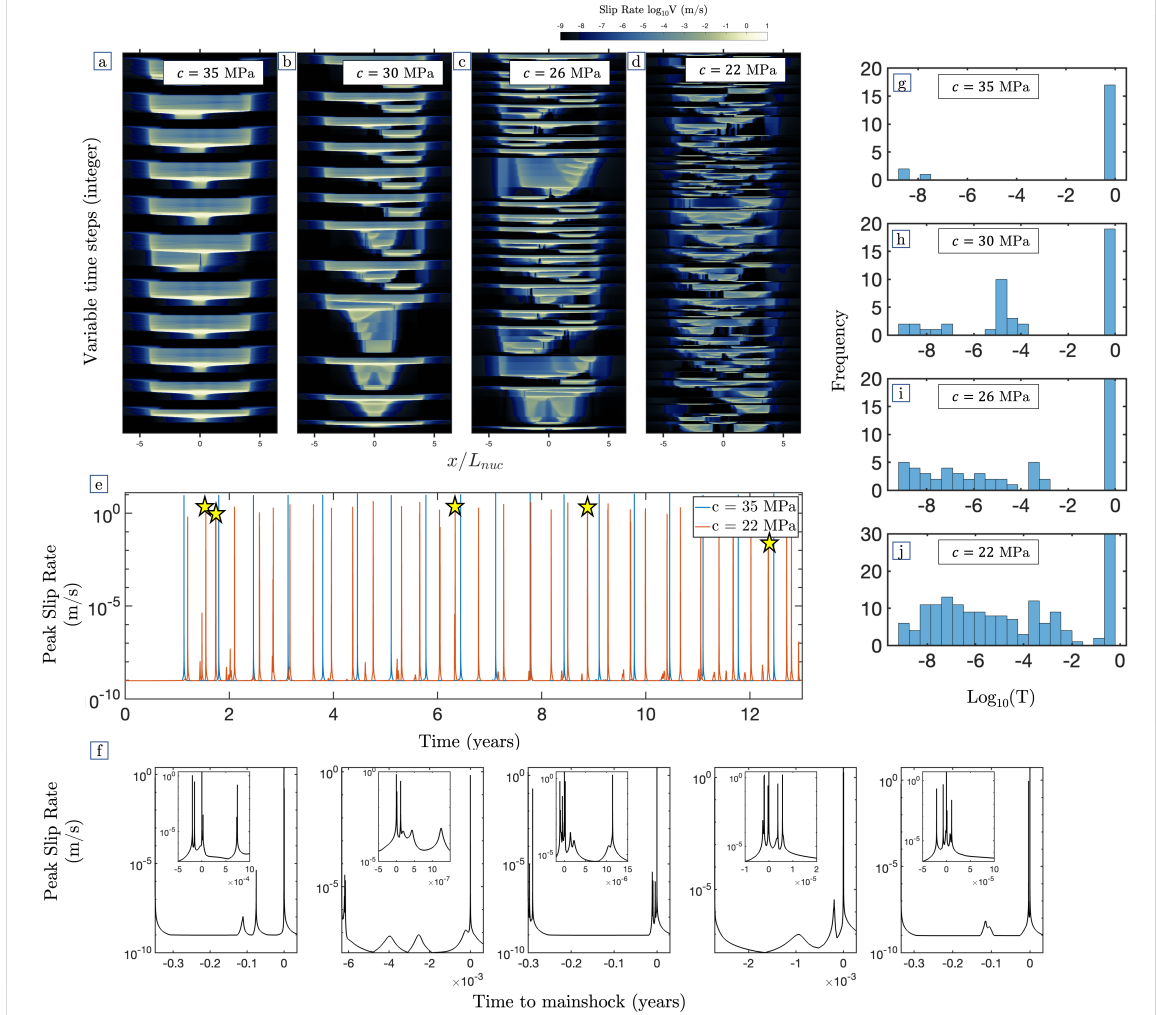


Figure 1: **Sequence of earthquakes and aseismic slip on a 2D in-plane rate-and-state fault.** (a-d) slip rate evolution with viscoplastic rheology illustrating increasing seismic complexity from periodic cycles to aperiodic sequence with segmented and partial ruptures as cohesion is reduced. (e) time history of the peak slip rate comparing $c = 35$ MPa with $c = 22$ MPa showing emergence of foreshocks and overall changes in recurrence pattern. (f) Time history panels showing foreshock patterns prior to mainshocks for several events highlighted by a yellow star in panel e. The zoomed in panels show individual event complexity. (g-j) Frequency distribution of interevent times highlighting the clustering behavior with reduction in bulk strength.

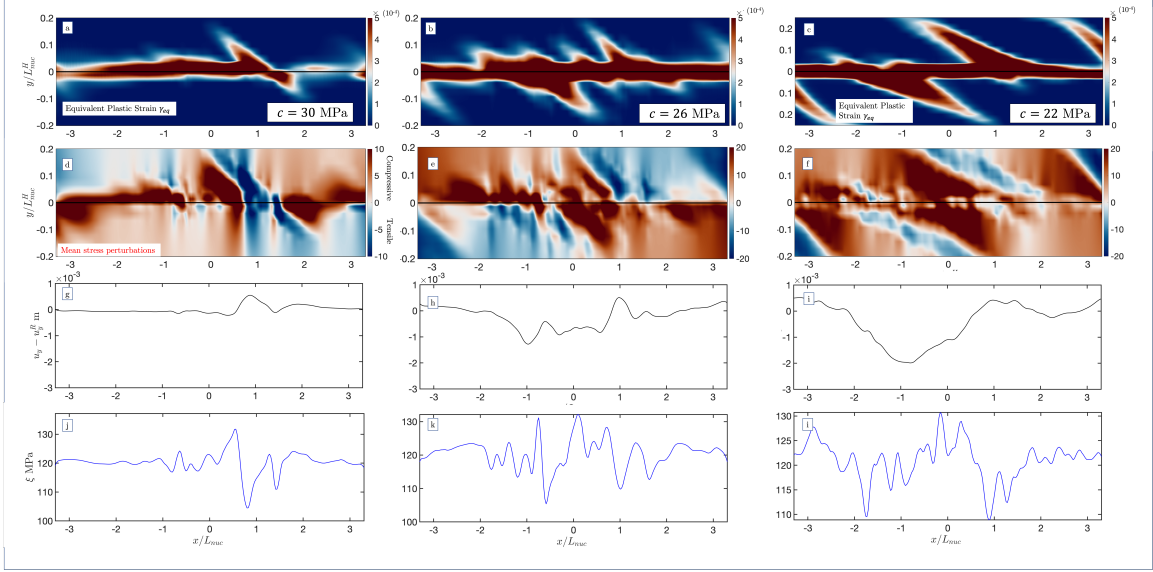


Figure 2: (a-c) The magnitude and extent of the equivalent plastic strain for three different cases of bulk cohesion $c = 30, 26,$ and 22 MPa at the end of the simulation showing varying patterns of accumulation based on the choice of bulk strength. (d-f) The mean stress distribution within the fault zone at the end of the earthquake cycle illustrating different evolution patterns based on the accumulated plasticity and seismic complexity. (g-i) The fault surface profile without the rotational component at the end of the cycle showing the emergence of short wave length fluctuations associated with fault zone structure evolution. (j-l) Associated changes in the normal stress on the fault demonstrating variations despite the planarity of the fault.

183 3.2 Evolution of Stress and Fault Structure

184 Simulations of single earthquakes demonstrate that the accumulation of plastic strain follows
 185 a specific pattern that is dictated by the choice of the angle of maximum compressive stress
 186 [44]. For the choices of $\Psi = 45^\circ$ the expected pattern of co-seismic plasticity is a fan-like
 187 distribution within the extensional quadrant of the bulk, defined by the sense of motion of
 188 the rupture front. In our analysis of sequences of earthquakes and aseismic slip, we instead
 189 observe a deviation from this expected pattern. Figure 2a-c show that at the end of the seismic
 190 sequence, the inelastic strain distribution is more broadly distributed in the near-fault region and
 191 accumulates on both sides of the fault. As discussed in [45], in addition, to rupture directivity,
 192 the accumulation of plastic strain in SEAS models is dictated by two other mechanisms. First,
 193 aseismic deformations induce changes in the mean stress field σ_m which influence the yield
 194 surface and create regions with lower mean stress that could favor plastic strain accumulation
 195 in subsequent dynamic ruptures. Also aseismic deformations may generate their own plasticity
 196 if the quasi-static stress concentration associated with the creeping fronts become large enough.
 197 Second, plastic strain accumulation causes residual mean stress changes. Specifically, mean stress
 198 becomes more compressive in regions where plasticity accumulates on the extensional side [44].
 199 However, changes in mean stress alters the yield strength which in turn impacts the potential for
 200 subsequent plastic strain accumulation. As a result, there is a correlation between plastic strain
 201 distribution and mean stress evolution. Furthermore, the mean stress field evolves, throughout
 202 the cycle, into a strongly heterogeneous distribution with alternating pockets of tensile and
 203 compressive perturbations relative to the initial mean stress value as shown in Figure 2d-f.

204 The magnitude, extent, and spatial distribution of the plastic strain depend on the fault zone
 205 strength as shown in 2a-c. As cohesion decreases, the width of the plastic zone increases and
 206 the magnitude of plastic strain becomes higher. This also correlates with larger variations in the
 207 mean stress that extend over larger distances away from the fault as shown in 2a-c. Importantly,

208 though, we observe that the width of the plastic zone in all cases is substantially smaller than the
 209 overall fault length and is on the order of a fraction of the nucleation zone size with a maximum
 210 extent of $0.2L_{nuc}$ for $c = 22$ MPa, which is approximately 3% of the total fault length. It is
 211 also important to note that the region with the most extensive plasticity accumulation is even
 212 smaller. This suggests that the implications of near fault plasticity on seismicity and stress
 213 evolution is significant despite the limited spatial extent and motivates further high resolution
 214 studies in the extreme vicinity of fault surfaces to characterize such inelastic processes.

215 Figure 2g-i illustrates the fault profile at the end of the simulation corresponding to different
 216 values of bulk cohesion. The fault profile is given by the magnitude of the transverse displace-
 217 ment u_y computed at the fault surface $y = 0$. For a homogeneous linear elastic medium, one
 218 expects a planar fault undergoing shear rupture to only rotate but remain primarily planar. The
 219 inelastic bulk rheology, however, leads to the emergence of partial ruptures due to the abrupt
 220 pinning of ruptures as well as stress heterogeneity. This results in the development of short
 221 wavelength undulations in the fault profile as shown in Figure 2g-i. To capture the variation
 222 in fault geometry in Figures 2g-i we only show the fault profile relative to overall fault rota-
 223 tion u_y^R . The fault rotation is computed by linearly fitting a displacement profile between the
 224 displacement at the right and the left ends of the VW patch of the fault. The magnitude and
 225 distribution of the undulations, referenced above, vary based on the choice of cohesion. Specifi-
 226 cally, we observe that for lower bulk strength, the undulations are more pronounced. They have
 227 larger amplitudes and vary over shorter wavelengths. On the other hand, for higher cohesion
 228 (e.g. $c = 30$ MPa), the fault profile, corrected for global rotation, remains almost flat. The
 229 undulations evolve throughout the cycle and contribute to the evolution of stress fields within
 230 in the near-fault region. The magnitude of these undulations is comparable to field observa-
 231 tions[46]. This suggests that bulk plasticity, and possibly other inelastic processes, may provide
 232 a self-roughening mechanism for faults, that has been largely understudied, even in the absence
 233 of initial roughness. Indeed, the role of pre-existing fault roughness has been previously high-
 234 lighted in the development of earthquake cycle and stress heterogeneity [47]. While we have not
 235 explored the role of the fault surface evolution on the slip dynamics explicitly, which requires
 236 solving the governing equations in the updated geometric configuration at each time step, the
 237 observed dynamic self-roughening mechanism is expected to contribute to the complexity of the
 238 seismic cycle, and dynamic rupture propagation [30, 34, 47, 48]. This observation suggests it
 239 might be important to consider the role of geometric nonlinearity (i.e adapting geometries) in
 240 models of sequences of earthquakes and aseismic slip.

241 Tied to the evolution of the fault surface profile, Figure 2j-l shows the end results of a
 242 corresponding evolution in the regularized normal stress ξ along the fault surface. The spatial
 243 variation in the normal stress is attributed to the combined effect of the emergence of short
 244 wavelength undulations and the nonuniform accumulation of plastic strain that cause different
 245 sides of the fault to deform differently in the fault normal direction. Although the fault surface is
 246 assumed to be initially planar, the normal stress heterogeneity emerge spontaneously and evolve
 247 throughout the sequence of events. However, the characteristics of this heterogeneity depend on
 248 the bulk strength and the cohesion value. Specifically, lower bulk strength enables shorter wave
 249 length variation in the spatial distribution of the normal stress. The peak value of the normal
 250 stress, however, is similar for all three cases.

251 To further understand the temporal evolution of fault zone plasticity based on the choice
 252 of bulk strength, Figure 3a-c illustrates the time history of the average plastic strain evolution
 253 in the near-fault region for three cases of decreasing cohesion $c = 30, 26,$ and 22 MPa. As
 254 expected, the magnitude of the average equivalent plastic strain increase with decreasing bulk
 255 strength. Similarly, we observe that the plasticity accumulated during the aseismic portion of
 256 the earthquake cycle also increases with decreasing bulk strength. Initially, during the early
 257 stages of the cycle, aseismic accumulation occurs rapidly, and then increases slowly throughout
 258 the cycle. Furthermore, we observe that the partitioning of plastic strain between the coseismic

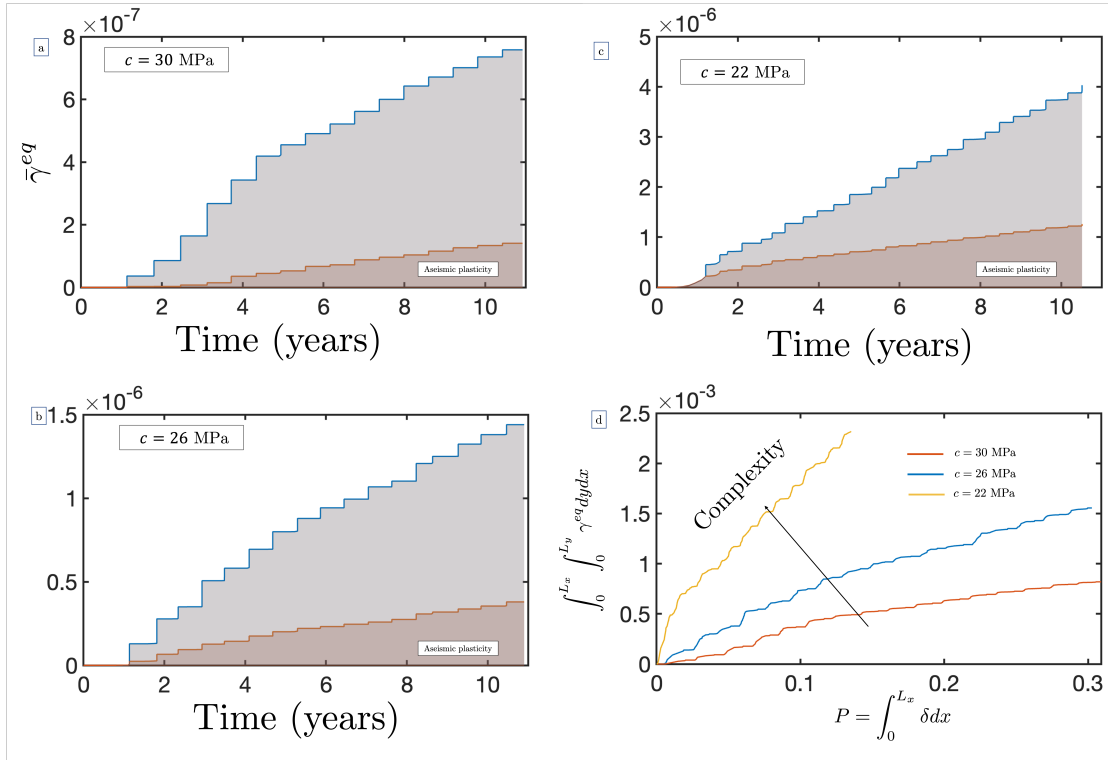


Figure 3: (a-b) Time history evolution of the average equivalent plastic strain within the off-fault bulk for three cases of different cohesion. Shading indicate partitioning between aseismic and coseismic plasticity. (d) The integrated equivalent plastic strain evolution with seismic potency indicating that complexity is associated with more bias toward off-fault deformations.

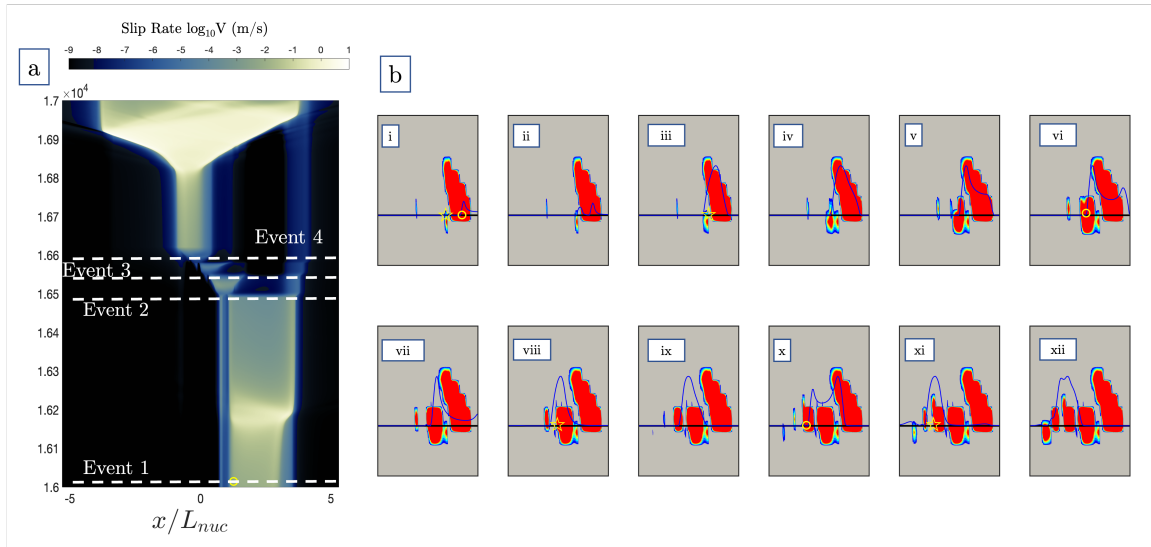


Figure 4: A specific snapshot for a cascading event presented for a case with cohesion $c = 30$ MPa. (a) The slip rate evolution for a viscoplastic 2-D fault illustrating cascading rupture propagation. (b) The partitioning between off-fault deformation and fault slip during this particular event sequence showing jerky rupture propagation in the form of individual events nucleation and arrest. The blue lines highlight the slip rate profile along the fault. The yellow circle indicate the location of rupture arrest, and the yellow star indicates the hypocenter of the renucleated rupture.

259 and aseismic phases also varies based on the choice of cohesion. As the cohesion decreases, a
 260 larger portion of overall plasticity accumulation is being accounted for aseismically. Specifically,
 261 by the end of the simulation, almost 19% of the total plastic strain is accumulated aseismically
 262 for $c = 30$ MPa. This fraction increased to 30% for $c = 22$ MPa. The increased role of aseismic
 263 plasticity partially explain the increased complexity in the seismicity and stress at lower bulk
 264 strength.

265 Finally, the partitioning of deformations between fault slip and off-fault plasticity plays a
 266 critical role in modulating the co-evolution of seismicity and fault zones. To highlight this, 3d
 267 shows the evolution of the integrated equivalent plastic strain within the near-fault region with
 268 fault slip expressed in terms of potency. There are two key observations: (1) the ratio between
 269 the integrated equivalent plastic strain and potency increases as the cohesion, and hence bulk
 270 strength, decreases, and (2) jumps associated with the increase in equivalent plastic strain are
 271 associated with minimal changes in potency. The first observation implies that complexity
 272 is proportional to the accumulation of plastic strain, with complexity being associated with
 273 more inelastic deformation delocalizing into the bulk. However, even for $c = 22$ MPa, the
 274 integrated equivalent plastic strain remain of the order of 1% of the seismic potency. The
 275 second observation suggests that there are periods during which it is more favorable for the
 276 deformation to be accommodated as bulk plasticity rather than fault slip. This, for example,
 277 may correspond to episodes of failed nucleation or arrested partial ruptures. In other words,
 278 these periods correspond to aseismic phases or episodes of transient slip deficit.

279 3.3 Cascading Earthquakes

280 Within our earthquake sequence with off-fault plasticity we observe the emergence of cascading
 281 earthquakes. These earthquakes just rupture, individually, a segment of the fault before
 282 arresting due to off-fault deformations. Nevertheless, due to a combination of (1) the favorable
 283 stress state and (2) the continuous creeping that concentrates the stress ahead of the pinned

284 rupture, subsequent earthquakes persistently nucleate along various segments of the fault in a
 285 brief timeframe, leading up to the eventual activation of the entire fault. Figure 4a shows the
 286 a cascading event sequence that occur for the case with cohesion $c = 30$ MPa. We observe
 287 the complexity of the earthquake sequence described above. Initially the rupture nucleates on
 288 the right side of the fault $x/L_{nuc} = 2.5$, the rupture propagate bilaterally prior to arresting
 289 due to inelastic strain accumulation. Eventually the stress concentration ahead of the pinned
 290 rupture tip is sufficient to trigger another rupture, which initiates ahead of the arrested event
 291 and rupture a new segment of the fault. This pattern keeps repeating with the triggering of
 292 event 3, and 4. Event 4 eventually rupture the whole seismogenic zone.

293 Figure 4c shows the rupture propagation as well as the pattern of plasticity accumulation
 294 within the bulk at different time steps within the cascading sequence of events. In panel (i-ii) We
 295 observe the onset of rupture arrest marked by the yellow circle accompanied by a substantial
 296 accumulation of off-fault plasticity. Within the same panel we highlight the location where
 297 the subsequent event will be triggered by a yellow star. The subsequent event is triggered
 298 ahead of the previously arrested panel as shown in panel (iii). In the intermediate panels (iii-v)
 299 the rupture proceeds to propagate prior to arresting in panel (vi) due to the accumulation of
 300 substantial inelastic strains. This pattern repeats again for the new ruptures that nucleates in
 301 panel (viii), and panel (xi).

302 This observed behavior is qualitatively similar to what has been observed in the quasi-static
 303 mode I fracture of elastic, perfectly plastic material in the plane strain configuration using the
 304 phase field approach[49]. Phase field models revealed that a plastic zone dulls the tip of a notch
 305 or crack, thereby impeding the initiation and spreading of the crack. When subjected to an
 306 adequate load, the crack initiates or unpins, but this occurs with a finite jump. As a result,
 307 the propagation is sporadic or abrupt, resulting in a rough surface. This jerky motion seems to
 308 persist for mode II dynamic fractures as observed here in our simulations suggesting a universal
 309 signature in elasto-plastic fracture phenomena.

310 4 Discussion

311 Our results indicate the accumulation of aseismic and coseismic off-fault deformation within the
 312 fault zone interact strongly with slip accumulation on the fault surface resulting in variations in
 313 the seismicity and stress patterns. In this work, we show that changing the bulk strength alters
 314 the earthquake sequence to produce complex slip patterns that depend on the extent of plastic
 315 strain accumulation. Based on the choice of bulk strength the fault surface exhibit a plethora of
 316 complex behavior such as partial ruptures, slow events, and intermittent episodes of earthquakes.
 317 The spatiotemporal complexity observed in our models is not tied to the particular choice of
 318 fault size[50], geometry[47] or heterogeneous distribution of frictional parameters. Rather, this
 319 complexity is attributed to the partitioning of deformation between fault slip and inelastic
 320 deformation in the bulk.

321 We have shown that plasticity accumulation produces persistent changes to the background
 322 stress field that influence the long term fault zone evolution and leads to emergence of regions
 323 of alternating compressive and tensile perturbations in the mean stress. Furthermore, our simu-
 324 lations highlight the role of bulk plasticity in the evolution of fault roughness and consequently
 325 short wavelength variations in the fault normal stress. These observations are consistent with
 326 recent experimental findings demonstrating that the sudden slip transition (in this particular
 327 case: the pinning of rupture tip) may produce substantial off-fault deformations and alter the
 328 fault surface in the fault normal direction [19].

329 Furthermore, we observe that the accumulation of off-fault inelastic deformations can lead to
 330 cascading sequence of events. This is due to accumulation of plastic zone which dulls the tip of
 331 the rupture front, thereby impeding the initiation and spreading of the rupture. Subjected to an
 332 sufficient load the rupture renucleate, however, with a finite jump. Consequently, the rupture

333 propagation becomes jerky, and within a short period of time (shorter than the recurrence
334 interval) several segments of the fault rupture independently. We note here that in the presence
335 of inelastic deformations we don't require any particular scaling of the fracture energy. Smaller
336 events are a direct consequence of more plastic dissipation and prior slip history, which eliminate
337 the need for fracture energy scaling (Gabriel et al., 2023) to achieve cascading events [51].
338 Furthermore, this study shows cascading events on a single fault that undergoes geometrical
339 and stress state evolution due to off-fault plasticity over seismic cycles. This observation of
340 cascading events is different from other cascading mechanisms involving elastic stress transfer
341 in fault segments or a network of faults [52–54].

342 We note that we have not studied very low cohesion values due to numerical instabilities
343 that emerge with the plasticity accumulation during the aseismic phases of the cycle prior to any
344 coseismic activity. However, recent work by Mia et al 2023, for antiplane deformations reveals
345 that as the rock strength is further reduced, the fault transitions into slow slip and seismicity
346 eventually shut off[39]. This limit remains to be studied in the in-plane case where aseismic
347 deformations can introduce mean stress perturbations and shift the yield envelope.

348 The main conclusions are summarized as follows:

- 349 1. Incorporating off-fault plasticity enable a transition from simple periodic through-going
350 events for higher bulk strength to chaotic sequences that exhibit temporal clustering and
351 spatial segmentation in the limit of lower bulk strength.
- 352 2. Accumulation of off-fault plasticity and emergence of partial ruptures lead to the evolution
353 of spatially heterogeneous normal stress field on the fault surface with short wavelength
354 variations, as well as, non-planar fault surface profile. For lower bulk strength, the fault
355 surface develop shorter wavelength undulations.
- 356 3. The overall plastic strain increases with decreasing bulk strength. The fraction of plastic
357 strain accumulated aseismically also increases with decreasing bulk strength.
- 358 4. The ratio between integrated plastic strain and potency increases with decreasing bulk
359 strength suggesting that a key mechanism for complex evolution of seismicity and stress
360 in fault zones lies in delocalizing of deformations. Lower bulk strength facilitates this
361 delocalization.
- 362 5. The extent of the fault zone that is plastically deforming remains very small compared to
363 the overall fault length. The ratio between the integrated plastic strain and potency is
364 also below 1% even for the lowest cohesion value considered in this study. Nonetheless,
365 the impact of bulk plasticity on seismicity and stresses is significant. This suggests the
366 need for further high resolution studies to characterize the complex near-fault response.
- 367 6. Off-fault plasticity present a possible mechanism for generating cascading earthquakes
368 without the need for fracture energy scaling. Cascading earthquakes and temporal cluster-
369 ing of earthquakes have been recently observed during the 2023 Herat earthquake sequence
370 [55]

371 **Acknowledgment**

372 M.A. would like to thank Ares Rosakis for insightful discussions. M.A. also acknowledges support
373 by the Caltech/MCE Big Ideas Fund (BIF), as well as the Caltech Terrestrial Hazard Obser-
374 vation and Reporting Center (THOR). The authors acknowledge support from the Southern
375 California Earthquake Center through a collaborative agreement between NSF. Grant Number:
376 EAR0529922 and USGS. Grant Number: 07HQAG0008 and the National Science Foundation
377 CAREER award No. 1753249 for modeling complex fault zone structures. This material is based
378 upon work supported by the Department of Energy under Award Number DE-FE0031685.

379 Data Availability

380 The authors accept AGU's data policy. Data generated from numerical simulations are uploaded
381 on CALTECH DATA repository and available online at <https://data.caltech.edu/records/nvvnq-qsg61>.
382

383 References

- 384 1. Chester, F. M., Evans, J. P. & Biegel, R. L. Internal structure and weakening mechanisms
385 of the San Andreas Fault. *Journal of Geophysical Research: Solid Earth* **98**, 771–786. ISSN:
386 01480227. <http://doi.wiley.com/10.1029/92JB01866> (Jan. 1993).
- 387 2. Mitchell, T. M. & Faulkner, D. R. The nature and origin of off-fault damage surrounding
388 strike-slip fault zones with a wide range of displacements: A field study from the Atacama
389 fault system, northern Chile. *Journal of Structural Geology* **31**, 802–816. ISSN: 01918141.
390 <http://dx.doi.org/10.1016/j.jsg.2009.05.002> (2009).
- 391 3. Huang, Y., Ampuero, J.-P. & Helmberger, D. V. Earthquake ruptures modulated by waves
392 in damaged fault zones. *Journal of Geophysical Research: Solid Earth* **119**, 3133–3154.
393 ISSN: 21699313. <http://doi.wiley.com/10.1002/2013JB010724> (Apr. 2014).
- 394 4. Huang, Y., Beroza, G. C. & Ellsworth, W. L. Stress drop estimates of potentially induced
395 earthquakes in the Guy-Greenbrier sequence. *Journal of Geophysical Research: Solid Earth*
396 **121**, 6597–6607. ISSN: 21699313. <http://doi.wiley.com/10.1002/2016JB013067> (Sept.
397 2016).
- 398 5. Barbot, S., Fialko, Y. & Sandwell, D. Effect of a compliant fault zone on the inferred
399 earthquake slip distribution. *Journal of Geophysical Research: Solid Earth* **113**, 1–10. ISSN:
400 21699356 (2008).
- 401 6. Lewis, M. A. & Ben-Zion, Y. Diversity of fault zone damage and trapping structures in
402 the Parkfield section of the San Andreas Fault from comprehensive analysis of near fault
403 seismograms. *Geophysical Journal International* **183**, 1579–1595. ISSN: 0956540X. [https:
404 //academic.oup.com/gji/article-lookup/doi/10.1111/j.1365-246X.2010.04816.x](https://academic.oup.com/gji/article-lookup/doi/10.1111/j.1365-246X.2010.04816.x)
405 (Dec. 2010).
- 406 7. Y.-G. Li & Leary, P. C. Fault zone trapped seismic waves. *Bulletin of the Seismological*
407 *Society of America* **80**, 1245–127 (1990).
- 408 8. Savage, H. M. & Brodsky, E. E. Collateral damage: Evolution with displacement of fracture
409 distribution and secondary fault strands in fault damage zones. *Journal of Geophysical*
410 *Research: Solid Earth* **116**. ISSN: 21699356 (Mar. 2011).
- 411 9. Biegel, R. L. & Sammis, C. G. *Relating Fault Mechanics to Fault Zone Structure* 2004.
- 412 10. Faulkner, D. R., Lewis, A. C. & Rutter, E. H. On the internal structure and mechanics
413 of large strike-slip fault zones: Field observations of the Carboneras fault in southeastern
414 Spain. *Tectonophysics* **367**, 235–251. ISSN: 00401951 (June 2003).
- 415 11. Weigandt, C., Griffith, W. & Rockwell, T. Role of confinement in coseismic pulveriza-
416 tion: Testing the rock record of rupture directivity on the San Jacinto fault, Southern
417 California. *Journal of Structural Geology* **177**, 104999. ISSN: 0191-8141. [https://www.
418 sciencedirect.com/science/article/pii/S019181412300216X](https://www.sciencedirect.com/science/article/pii/S019181412300216X) (2023).
- 419 12. Huang, Y., Ampuero, J.-P. & Helmberger, D. V. Earthquake ruptures modulated by waves
420 in damaged fault zones. *Journal of Geophysical Research: Solid Earth* **119**, 3133–3154.
421 eprint: <https://agupubs.onlinelibrary.wiley.com/doi/pdf/10.1002/2013JB010724>.
422 <https://agupubs.onlinelibrary.wiley.com/doi/abs/10.1002/2013JB010724> (2014).

- 423 13. Smith, Z. D. & Griffith, W. A. Evolution of Pulverized Fault Zone Rocks by Dynamic Ten-
424 sile Loading During Successive Earthquakes. *Geophysical Research Letters* **49**. e2022GL099971
425 2022GL099971, e2022GL099971. eprint: [https://agupubs.onlinelibrary.wiley.com/
426 doi/pdf/10.1029/2022GL099971](https://agupubs.onlinelibrary.wiley.com/doi/pdf/10.1029/2022GL099971). [https://agupubs.onlinelibrary.wiley.com/doi/
427 abs/10.1029/2022GL099971](https://agupubs.onlinelibrary.wiley.com/doi/abs/10.1029/2022GL099971) (2022).
- 428 14. Ben-Zion, Y. & Ampuero, J.-P. Seismic radiation from regions sustaining material damage.
429 *Geophysical Journal International* **178**, 1351–1356. ISSN: 0956-540X. eprint: [https://
430 academic.oup.com/gji/article-pdf/178/3/1351/5871906/178-3-1351.pdf](https://academic.oup.com/gji/article-pdf/178/3/1351/5871906/178-3-1351.pdf). [https://
431 //doi.org/10.1111/j.1365-246X.2009.04285.x](https://doi.org/10.1111/j.1365-246X.2009.04285.x) (Sept. 2009).
- 432 15. Ben-Zion, Y. & Lyakhovsky, V. Representation of seismic sources sustaining changes of
433 elastic moduli. *Geophysical Journal International* **217**, 135–139. ISSN: 0956-540X. eprint:
434 <https://academic.oup.com/gji/article-pdf/217/1/135/27662171/ggz018.pdf>.
435 <https://doi.org/10.1093/gji/ggz018> (Jan. 2019).
- 436 16. Lyakhovsky, V. & Ben-Zion, Y. Isotropic seismic radiation from rock damage and dila-
437 tancy. *Geophysical Journal International* **222**, 449–460. ISSN: 0956-540X. eprint: [https://
438 //academic.oup.com/gji/article-pdf/222/1/449/33181717/ggaa176.pdf](https://academic.oup.com/gji/article-pdf/222/1/449/33181717/ggaa176.pdf). [https://
439 //doi.org/10.1093/gji/ggaa176](https://doi.org/10.1093/gji/ggaa176) (Apr. 2020).
- 440 17. Kwiatek, G. & Ben-Zion, Y. Assessment of P and S wave energy radiated from very small
441 shear-tensile seismic events in a deep South African mine. *Journal of Geophysical Research:
442 Solid Earth* **118**, 3630–3641. eprint: [https://agupubs.onlinelibrary.wiley.com/doi/
443 pdf/10.1002/jgrb.50274](https://agupubs.onlinelibrary.wiley.com/doi/pdf/10.1002/jgrb.50274). [https://agupubs.onlinelibrary.wiley.com/doi/abs/10.
444 1002/jgrb.50274](https://agupubs.onlinelibrary.wiley.com/doi/abs/10.1002/jgrb.50274) (2013).
- 445 18. Cheng, Y., Wang, X., Zhan, Z. & Ben-Zion, Y. Isotropic Source Components of Events in
446 the 2019 Ridgecrest, California, Earthquake Sequence. *Geophysical Research Letters* **48**.
447 e2021GL094515 2021GL094515, e2021GL094515. eprint: [https://agupubs.onlinelibrary.
448 wiley.com/doi/pdf/10.1029/2021GL094515](https://agupubs.onlinelibrary.wiley.com/doi/pdf/10.1029/2021GL094515). [https://agupubs.onlinelibrary.
449 wiley.com/doi/abs/10.1029/2021GL094515](https://agupubs.onlinelibrary.wiley.com/doi/abs/10.1029/2021GL094515) (2021).
- 450 19. Ross, E. O., Reber, J. E. & Titus, S. J. Relating Slip Behavior to Off-Fault Deformation
451 Using Physical Models. *Geophysical Research Letters* **49**. ISSN: 0094-8276 (June 2022).
- 452 20. Ben-Zion, Y. & Sammis, C. G. Characterization of fault zones. *Pure and Applied Geophysics*
453 **160**, 677–715. ISSN: 00334553 (2003).
- 454 21. Abdelmeguid, M. & Elbanna, A. Modeling Sequences of Earthquakes and Aseismic Slip
455 (SEAS) in Elasto-Plastic Fault Zones With a Hybrid Finite Element Spectral Bound-
456 ary Integral Scheme. *Journal of Geophysical Research: Solid Earth* **127**. e2022JB024548
457 2022JB024548, e2022JB024548. eprint: [https://agupubs.onlinelibrary.wiley.com/
458 doi/pdf/10.1029/2022JB024548](https://agupubs.onlinelibrary.wiley.com/doi/pdf/10.1029/2022JB024548). [https://agupubs.onlinelibrary.wiley.com/doi/
459 abs/10.1029/2022JB024548](https://agupubs.onlinelibrary.wiley.com/doi/abs/10.1029/2022JB024548) (2022).
- 460 22. Rice, J. R., Sammis, C. G. & Parsons, R. Off-fault secondary failure induced by a dynamic
461 slip pulse. *Bulletin of the Seismological Society of America* **95**, 109–134. ISSN: 00371106
462 (Feb. 2005).
- 463 23. Mitchell, T. M. & Faulkner, D. R. Towards quantifying the matrix permeability of fault
464 damage zones in low porosity rocks. *Earth and Planetary Science Letters* **339-340**, 24–31.
465 ISSN: 0012821X (July 2012).
- 466 24. Childs, C. *et al.* A geometric model of fault zone and fault rock thickness variations. *Journal*
467 *of Structural Geology* **31**, 117–127. ISSN: 01918141 (Feb. 2009).

- 468 25. Heap, M. J., Faulkner, D. R., Meredith, P. G. & Vinciguerra, S. Elastic moduli evolution
469 and accompanying stress changes with increasing crack damage: Implications for stress
470 changes around fault zones and volcanoes during deformation. *Geophysical Journal Inter-*
471 *national* **183**, 225–236. ISSN: 0956540X (Oct. 2010).
- 472 26. Chester, J. S., Chester, F. M. & Kronenberg, A. K. Fracture surface energy of the Punch-
473 bowl fault, San Andreas system. *Nature* **437**, 133–136. ISSN: 0028-0836. <http://www.nature.com/articles/nature03942> (Sept. 2005).
474
- 475 27. Griffith, W. A., Nielsen, S., Di Toro, G. & Smith, S. A. Rough faults, distributed weak-
476 ening, and off-fault deformation. *Journal of Geophysical Research: Solid Earth* **115**. ISSN:
477 21699356 (Aug. 2010).
- 478 28. Mutlu, O. & Pollard, D. D. On the patterns of wing cracks along an outcrop scale flaw:
479 A numerical modeling approach using complementarity. *Journal of Geophysical Research:*
480 *Solid Earth* **113**. ISSN: 21699356 (June 2008).
- 481 29. Manighetti, I., King, G. & Sammis, C. G. The role of off-fault damage in the evolution of
482 normal faults. *Earth and Planetary Science Letters* **217**, 399–408. ISSN: 0012821X. <https://linkinghub.elsevier.com/retrieve/pii/S0012821X03006010> (Jan. 2004).
483
- 484 30. Tal, Y. & Faulkner, D. The Effect of Fault Roughness and Earthquake Ruptures on the
485 Evolution and Scaling of Fault Damage Zones. *Journal of Geophysical Research: Solid Earth*
486 **127**. ISSN: 2169-9313 (Jan. 2022).
- 487 31. Perrin, C., Manighetti, I., Ampuero, J. P., Cappa, F. & Gaudemer, Y. Location of largest
488 earthquake slip and fast rupture controlled by along-strike change in fault structural ma-
489 turity due to fault growth. *Journal of Geophysical Research: Solid Earth* **121**, 3666–3685.
490 ISSN: 21699356 (May 2016).
- 491 32. Faulkner, D. R., Mitchell, T. M., Jensen, E. & Cembrano, J. Scaling of fault damage zones
492 with displacement and the implications for fault growth processes. *Journal of Geophysical*
493 *Research: Solid Earth* **116**. ISSN: 21699356 (May 2011).
- 494 33. Anders, M. H. & Wiltschko, D. V. *Microfracturing, paleostress and the growth of faults*
495 tech. rep. 6 (1994), 795.
- 496 34. Dunham, E. M., Belanger, D., Cong, L. & Kozdon, J. E. Earthquake ruptures with strongly
497 rate-weakening friction and off-fault plasticity, part 1: Planar faults. *Bulletin of the Seis-*
498 *mological Society of America* **101**, 2296–2307. ISSN: 00371106 (2011).
- 499 35. Huang, Y. & Ampuero, J.-P. Pulse-like ruptures induced by low-velocity fault zones. *Jour-*
500 *nal of Geophysical Research* **116**, B12307. ISSN: 0148-0227. [http://doi.wiley.com/10.](http://doi.wiley.com/10.1029/2011JB008684)
501 [1029/2011JB008684](http://doi.wiley.com/10.1029/2011JB008684) (Dec. 2011).
- 502 36. Thakur, P., Huang, Y. & Kaneko, Y. Effects of Low-Velocity Fault Damage Zones on Long-
503 Term Earthquake Behaviors on Mature Strike-Slip Faults. *Journal of Geophysical Research:*
504 *Solid Earth* **125**, 1–20. ISSN: 21699356 (2020).
- 505 37. Erickson, B. A., Dunham, E. M. & Khosravifar, A. A finite difference method for off-fault
506 plasticity throughout the earthquake cycle. *Journal of the Mechanics and Physics of Solids*
507 **109**, 50–77. ISSN: 00225096. <http://dx.doi.org/10.1016/j.jmps.2017.08.002> (2017).
- 508 38. Mia, M. S., Abdelmeguid, M. & Elbanna, A. E. Spatio-Temporal Clustering of Seismicity
509 Enabled by Off-Fault Plasticity. *Geophysical Research Letters* **49**. ISSN: 19448007 (Apr.
510 2022).
- 511 39. Mia, M. S., Abdelmeguid, M. & Elbanna, A. E. The spectrum of fault slip in elastoplastic
512 fault zones. *Earth and Planetary Science Letters* **619**, 118310. ISSN: 0012-821X. <https://www.sciencedirect.com/science/article/pii/S0012821X23003230> (2023).
513

- 514 40. Cochard, A. & Rice, J. R. Fault rupture between dissimilar materials: Ill-posedness, reg-
515 ularization, and slip-pulse response. *Journal of Geophysical Research: Solid Earth* **105**,
516 25891–25907. ISSN: 01480227. <http://doi.wiley.com/10.1029/2000JB900230> (Nov.
517 2000).
- 518 41. Ranjith, K. & Rice, J. R. *Slip dynamics at an interface between dissimilar materials* tech.
519 rep. (2001), 341–361. www.elsevier.com/locate/jmps.
- 520 42. Tal, Y., Rubino, V., Rosakis, A. J. & Lapusta, N. Illuminating the physics of dynamic fric-
521 tion through laboratory earthquakes on thrust faults. *Proceedings of the National Academy*
522 *of Sciences* **117**, 21095–21100. ISSN: 0027-8424. [http://www.pnas.org/lookup/doi/10.](http://www.pnas.org/lookup/doi/10.1073/pnas.2004590117)
523 [1073/pnas.2004590117](http://www.pnas.org/lookup/doi/10.1073/pnas.2004590117) (Sept. 2020).
- 524 43. Abdelmeguid, M., Ma, X. & Elbanna, A. A Novel Hybrid Finite Element-Spectral Boundary
525 Integral Scheme for Modeling Earthquake Cycles: Application to Rate and State Faults
526 With Low-Velocity Zones. *Journal of Geophysical Research: Solid Earth* **124**, 12854–12881.
527 ISSN: 21699356 (Dec. 2019).
- 528 44. Templeton, E. L. & Rice, J. R. Off-fault plasticity and earthquake rupture dynamics: 1.
529 Dry materials or neglect of fluid pressure changes. *Journal of Geophysical Research: Solid*
530 *Earth* **113**, 1–19. ISSN: 21699356 (2008).
- 531 45. Abdelmeguid, M. & Elbanna, A. Modeling Sequences of Earthquakes and Aseismic Slip
532 (SEAS) in Elasto-plastic Fault Zones with A Hybrid Finite Element Spectral Boundary
533 Integral scheme. <https://doi.org/10.1002/essoar.10511050.2>.
- 534 46. Renard, F. & Candela, T. in *Fault Zone Dynamic Processes* 195–215 (American Geophys-
535 ical Union (AGU), 2017). ISBN: 9781119156895. eprint: [https://agupubs.onlinelibrary.](https://agupubs.onlinelibrary.wiley.com/doi/pdf/10.1002/9781119156895.ch10)
536 [wiley.com/doi/pdf/10.1002/9781119156895.ch10](https://agupubs.onlinelibrary.wiley.com/doi/pdf/10.1002/9781119156895.ch10). [https://agupubs.onlinelibrary.](https://agupubs.onlinelibrary.wiley.com/doi/abs/10.1002/9781119156895.ch10)
537 [wiley.com/doi/abs/10.1002/9781119156895.ch10](https://agupubs.onlinelibrary.wiley.com/doi/abs/10.1002/9781119156895.ch10).
- 538 47. Cattania, C. & Segall, P. Precursory Slow Slip and Foreshocks on Rough Faults. *Journal*
539 *of Geophysical Research: Solid Earth* **126**. ISSN: 21699356 (Apr. 2021).
- 540 48. Romanet, P. & Ozawa, S. Fully Dynamic Earthquake Cycle Simulations on a Nonplanar
541 Fault Using the Spectral Boundary Integral Element Method (sBIEM). *Bulletin of the*
542 *Seismological Society of America* **112**, 78–97. ISSN: 0037-1106. eprint: [https://pubs.](https://pubs.geoscienceworld.org/ssa/bssa/article-pdf/112/1/78/5518864/bssa-2021178.1.pdf)
543 [geoscienceworld.org/ssa/bssa/article-pdf/112/1/78/5518864/bssa-2021178.1.](https://pubs.geoscienceworld.org/ssa/bssa/article-pdf/112/1/78/5518864/bssa-2021178.1.pdf)
544 [pdf](https://pubs.geoscienceworld.org/ssa/bssa/article-pdf/112/1/78/5518864/bssa-2021178.1.pdf). <https://doi.org/10.1785/0120210178> (Oct. 2021).
- 545 49. Brach, S., Tanné, E., Bourdin, B. & Bhattacharya, K. Phase-field study of crack nucleation
546 and propagation in elastic–perfectly plastic bodies. *Computer Methods in Applied Mechan-*
547 *ics and Engineering* **353**, 44–65. ISSN: 0045-7825. [https://www.sciencedirect.com/](https://www.sciencedirect.com/science/article/pii/S0045782519302300)
548 [science/article/pii/S0045782519302300](https://www.sciencedirect.com/science/article/pii/S0045782519302300) (2019).
- 549 50. Barbot, S. Modulation of fault strength during the seismic cycle by grain-size evolution
550 around contact junctions. *Tectonophysics* **765**, 129–145. ISSN: 00401951. [https://doi.](https://doi.org/10.1016/j.tecto.2019.05.004)
551 [org/10.1016/j.tecto.2019.05.004](https://doi.org/10.1016/j.tecto.2019.05.004) (2019).
- 552 51. Gabriel, A.-A., Garagash, D. I., Palgunadi, K. H. & Mai, P. M. *Fault-size dependent fracture*
553 *energy explains multi-scale seismicity and cascading earthquakes* 2023. arXiv: 2307.15201
554 [physics.geo-ph].
- 555 52. Palgunadi, K. H., Gabriel, A.-A., Garagash, D. I., Ulrich, T. & Mai, P. M. *Rupture Dynam-*
556 *ics of Cascading Earthquakes in a Multiscale Fracture Network* 2023. arXiv: 2307.14229
557 [physics.geo-ph].
- 558 53. Im, K. & Avouac, J.-P. Cascading foreshocks, aftershocks and earthquake swarms in a
559 discrete fault network. *Geophysical Journal International* **235**, 831–852. ISSN: 0956-540X.
560 eprint: [https://academic.oup.com/gji/article-pdf/235/1/831/50959708/ggad278.](https://academic.oup.com/gji/article-pdf/235/1/831/50959708/ggad278.pdf)
561 [pdf](https://academic.oup.com/gji/article-pdf/235/1/831/50959708/ggad278.pdf). <https://doi.org/10.1093/gji/ggad278> (July 2023).

- 562 54. Ozawa, S. & Ando, R. Mainshock and Aftershock Sequence Simulation in Geometrically
563 Complex Fault Zones. *Journal of Geophysical Research: Solid Earth* **126**. e2020JB020865
564 2020JB020865, e2020JB020865. eprint: [https://agupubs.onlinelibrary.wiley.com/
565 doi/pdf/10.1029/2020JB020865](https://agupubs.onlinelibrary.wiley.com/doi/pdf/10.1029/2020JB020865). [https://agupubs.onlinelibrary.wiley.com/doi/
566 abs/10.1029/2020JB020865](https://agupubs.onlinelibrary.wiley.com/doi/abs/10.1029/2020JB020865) (2021).
- 567 55. US Geological Survey. *M 6.3 - 34 km NNW of Herāt, Afghanistan* [https://earthquake.
568 usgs.gov/earthquakes/eventpage/us60001fn5/executive](https://earthquake.usgs.gov/earthquakes/eventpage/us60001fn5/executive).

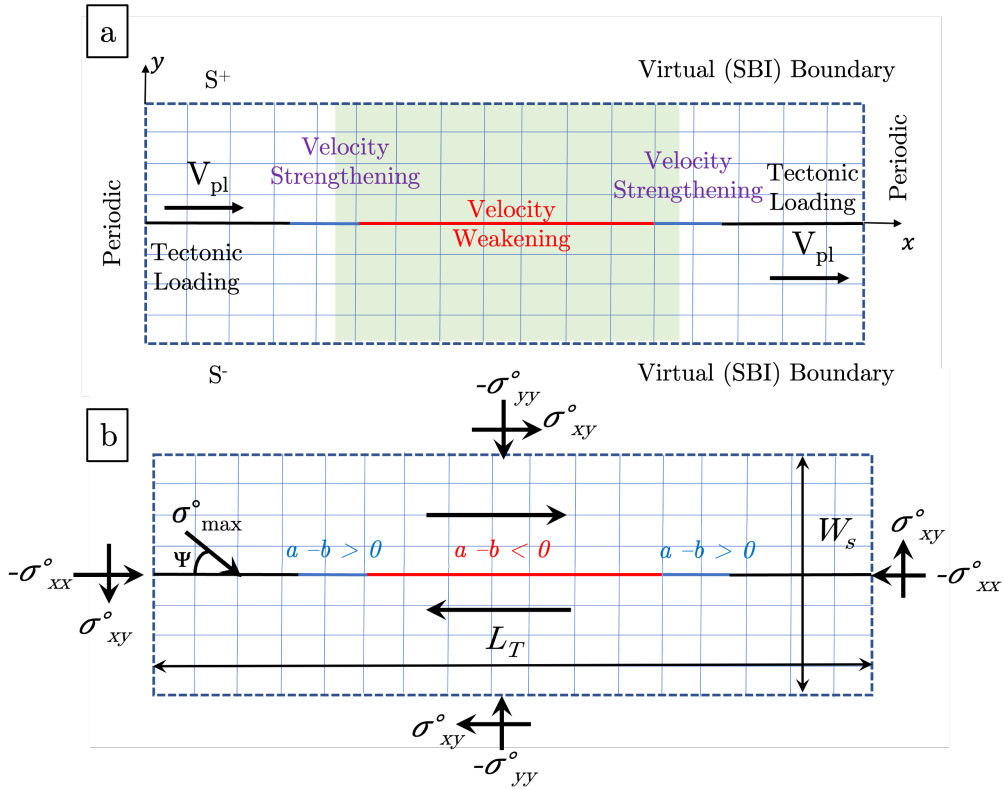


Figure A1: **Schematic of the model considered in this paper** (a) The computational setup for the hybrid FE-SBI scheme. A domain Ω adjacent to the fault surface is discretized using the finite element method. The spectral boundary integral method is utilized to model the external linearly elastic half spaces without explicit discretization. The response on the virtual boundaries parallel to the fault surface is expressed through an integral relation between the displacement and traction. Periodicity is imposed on the lateral boundaries of the domain. (b) The distribution of the fault frictional parameters and background tectonic stress field.

Table A1: Parameters description

Medium Parameter	Symbol	Value
Shear wave speed (km/s)	c_s	3.5
Pressure wave speed (km/s)	c_p	6.0
Density (kg/m ³)	ρ	2670.0
Length of the domain (m)	L_T	150
Distance between two virtual boundaries (m)	W_s	varies
Angle of Internal Friction	ϕ	31.6°
Cohesion MPa	c	varies
Angle of Maximum Compressive principal stress	Ψ	45°
Viscosity term (MPa-s)	η	0.32
Background Stress	Symbol	Value
Background Vertical Stress MPa	σ_{yy}	120
Background Horizontal Stress MPa	σ_{xx}	120
Background Shear Stress MPa	σ_{xy}	59.1
Fault Parameters	Symbol	Value
Static Coefficient of friction	f_o	0.6
Critical slip distance (μm)	L	50
Reference velocity (m/s)	V_o	10 ⁻⁶
Tectonic loading (m/s)	V_{pl}	10 ⁻⁹
Length of VW patch (m)	L_{VW}	50
Length of transition (m)	L_{VW-VS}	5
Length of the fault (m)	L_f	90
Evolution effect parameter	b	0.015
Steady state velocity dependence in VW patch	$(a_{VW} - b)$	-0.005
Steady state velocity dependence in VS patch	$(a_{VS} - b)$	0.015
Nucleation size (m)	L_{nuc}	6.96
Quasi-static process zone size (m)	L_b	1.2
Grid size (m)	Δx	0.1

On the Interplay between Distributed Bulk Plasticity and Local Fault Slip in Evolving Fault Zone Complexity

Mohamed Abdelmeguid^a, Md Shumon Mia^{b,c}, and Ahmed Elbanna^{b,d}

^aGraduate Aerospace Laboratories, California Institute of Technology, Pasadena, CA, USA.

^bDepartment of Civil and Environmental Engineering, University of Illinois at Urbana-Champaign, Urbana, IL, USA

^cDepartment of Mechanical Science and Engineering, University of Illinois at Urbana-Champaign, Urbana, IL, USA

^dBeckman Institute of Advanced Science and Technology, University of Illinois at Urbana-Champaign, Urbana, IL, USA,

*e-mail: meguid@caltech.edu

Key Points:

- Partitioning of deformation between bulk and fault contribute to seismic complexity.
- Seismic complexity and accumulation of plastic strain induce normal stress perturbations on the fault.
- Off-fault inelastic deformation result in cascading earthquake.

Abstract

We numerically investigate the role of plastic strain accumulation on the mechanical response of a planar strike-slip fault. Our models show that fault-zone strength significantly impact the ensuing sequence of earthquakes. Weaker fault zones accumulating more plastic strain promote more complexity in the seismicity pattern through aperiodic earthquake occurrences and intermittent episodes of rupture and arrest. However, if the fault zone strength is high enough, the overall earthquake sequence is characterized by periodic fault-spanning events. We find that both the fault normal stress and the fault surface profile evolve throughout the earthquake sequence, suggesting a self-roughening mechanism. Despite the significant impact of plasticity on the fault response, the width of the plastically deforming region in the fault zone is small compared to the fault length. Our results suggest a rich behavior in dynamically evolving fault zones and support the need for further high-resolution studies of the highly non-linear near-fault region.

Plain Language Summary

Why do some faults fail in large earthquakes while other faults generate smaller ones? In our computer simulation study, we explored how the strength of a strike-slip fault (where Earth's crust plates slide past each other) affects earthquake patterns. We discovered that weaker fault zones, which can stretch or squeeze more, often have more complex and unpredictable earthquake patterns, including irregular timings and smaller, clustered earthquakes. In contrast, stronger fault zones tend to have regular, larger earthquakes. Interestingly, in weaker fault zones, the geometry of the fault surface can change over time and become rougher in response to the

39 deformability of the surrounding rocks, suggesting a roughening of the fault surface. Although
40 these changes significantly influence earthquake patterns, they occur in a relatively small region
41 surrounding fault surfaces highlighting the need for expanding instrumentation closer to active
42 faults. These findings are useful for contextualizing observed seismicity patterns and are relevant
43 for seismic hazard studies.

44 1 Introduction

45 Geological observations of fault zones highlight a region of pervasive damage that surrounds
46 the principal slip surfaces [1–7]. A typical strike slip fault zone may have one or more fault
47 cores with damage features at varying length scales from fine scale distributed damage to more
48 discrete anisotropic secondary faults. In general, the distribution and intensity of damage decays
49 away from the main fault, leading to a gradual transition from a damaged zone to intact host
50 rock [2, 8]. Extensive studies on damaged fault zones reveal substantial differences between
51 the mechanical properties of the inner fault zone core compared to the host rock material [9,
52 10]. This variation in fault zone properties was found to influence many rupture characteristics
53 including rupture directivity [11], rupture speed, high frequency generation [12], maximum
54 event magnitude [13], radiation patterns [14–18] and surface deformation [19].

55 Fault zone damage may accumulate both seismically and aseismically [1, 2, 20, 21] and is
56 generally enhanced in the presence of geometrical complexity [22–30]. Prior studies suggest that
57 regardless of the damage generation mechanism, the scale of damage evolution varies based on
58 the maturity of the fault core [31]. Specifically, fault zone damage scales with fault slip up a
59 certain threshold above which the fault zone width growth is minimal [8, 32]. Furthermore, the
60 damage density decreases exponentially or as a power law with distance normal to the fault
61 surface [8, 26, 33].

62 Fault zone damage has been studied extensively using dynamic rupture simulations [34–36]
63 using different idealizations including plasticity theories and continuum damage mechanics as
64 well as the limiting case of an elastic low velocity fault zone. Among the major conclusions
65 of these studies are that the damage region contributes to a heterogeneous local stress field on
66 the fault, acts as an energy sink increasing the total energy dissipated during dynamic rupture,
67 and leads to generation of trapped waves that may enhance high frequency generation and
68 influence the rupture mode. While, dynamic rupture simulations provide significant insight
69 into the accumulation and effects of damage during earthquake rupture. Field observation
70 indicates that damage accumulation on larger faults is associated with overprinting from multiple
71 slip events rather than a single dynamic event. To this point, earthquake cycle simulations
72 that are capable of modeling sequences of earthquakes are a prime candidate for the study of
73 evolving damage profiles on a fault zone. However, due to the numerical complexity of modeling
74 multiple earthquakes over different spatial and temporal scales, only a handful of earthquake
75 cycle studies investigated the effect of the bulk material response, beyond elasticity [21, 30,
76 37–39]. In anti-plane approximation, [38] utilized a combined finite element spectral boundary
77 integral scheme (FEBE) to investigate the effects of the bulk yield strength on the overall
78 sequence of the earthquake and aseismic slip and the evolution of inelastic strain. In that study,
79 they demonstrated that the partitioning between off-fault deformations and fault slip could lead
80 to a complex sequence of seismicity. However, within that study, the role of pressure-dependent
81 rock strength was neglected. Recently, Abdelmeguid and Elbanna demonstrated, in the context
82 of 2D plane-strain approximation, that there is a feedback mechanism between the evolution
83 of plastic strain in the bulk and mean stress which in turn influences the pressure-dependent
84 yield strength and subsequent generation of plastic strain [21]. Accordingly, it still remains to
85 be investigated whether the spatio-temporal clustering observed in the anti-plane model would
86 persist in the context of in-plane deformations, and what role the feedback between mean stress
87 and inelastic strain accumulation plays in fault zone maturity.

88 In this paper, we focus on aspects related to the co-evolution of seismicity and off-fault
89 viscoplastic bulk rheology. We consider the 2D plane-strain approximation as a minimal model
90 that enables us to study the role of pressure-dependent plasticity. We use a hybrid finite element
91 spectral boundary integral framework, FEBE, which accounts for the full inertia effect during
92 the seismic phase and enables accurate near field truncation of the wave field. We study the
93 evolution of the sequence of earthquakes and aseismic slip for different choices of bulk strength
94 and implications for event size distribution, partitioning of deformation, stress heterogeneity,
95 and fault surface evolution. We outline the setup of the model and summarize the main results
96 in the next section

97 2 Model Description

98 We consider a planar horizontal fault, with a right-lateral sense of motion, the frictional be-
99 havior is governed by rate-and-state friction under a 2D plane strain approximation. The fault
100 is bisecting an unbounded elastic-visco-plastic domain with homogeneous elastic properties as
101 shown in Figure A1a. The fault consists of a central velocity weakening patch surrounded by two
102 velocity strengthening patches and is being loaded from both ends by a constant plate loading
103 rate as shown in Figure A1b. The initial prestress σ_{ij}^0 shown in Figure A1b is assumed to be
104 uniform.

105 The bulk is initially assumed to be linear elastic. We use pressure-dependent Drucker-Prager
106 (DP) plasticity to describe the inelastic bulk response beyond the onset of yielding. The DP
107 yield surface is parameterized by two parameters: the angle of internal friction ϕ and cohesion
108 c . We assume a non-associative flow rule and Perzyna type viscous regularization. We vary the
109 value of the cohesion parameter c to explore the effect of fault zone strength on the evolution of
110 seismicity and near fault stresses and deformations. We implement normal stress regularization
111 on the fault surface following Prakash-Clifton law that ensures the fault local frictional strength
112 is a function of the history of the normal stress on the fault and eliminates any spurious unstable
113 modes that may emerge due to rapid variations in the instantaneous value of the normal stress
114 [40–42].

115 We use the FEBE framework presented in [21, 43] to explore the co-interplay between local-
116 ized fault slip and distributed bulk inelastic deformations through long sequences of earthquakes
117 and aseismic slip (SEAS). FEBE is a hybrid finite element spectral boundary integral scheme.
118 Spatially, FEBE adopts a domain decomposition approach where the near fault region that in-
119 cludes the potentially nonlinear material response is discretized using the finite element method.
120 The exterior half spaces beyond the near fault region are assumed to be linear elastic and ho-
121 mogeneous and are thus described by a spectral boundary integral formulation. The fault zone
122 and the exterior half spaces are coupled through the enforcement of continuity of traction and
123 displacement at their interfaces. The local nature of near-fault nonlinearities ensures that the
124 width of the discretized region W_s (shown in Figure A1b) is usually much smaller than the total
125 domain length L_T . The FEM domain size is selected such that the discretized domain contains
126 all the off-fault plasticity. For planar faults previous studies on dynamic fracture with off-fault
127 plasticity suggest that the extent of the plastic zone is proportional to the process zone size, this
128 estimate guides our initial choice of W_s [34, 44].

129 Temporally, FEBE implements an alternating quasi-dynamic scheme, to resolve interseismic
130 slow deformation while neglecting inertia effects, and a fully dynamic scheme, to resolve rapid
131 seismic periods while accounting for fully inertia effects. The switch between the two schemes is
132 determined by a velocity threshold. More details about the numerical algorithm may be found
133 in Abdelmeguid and Elbanna 2022 [21]. The values of the different parameters used in the model
134 are summarized in Table A1

3 Results

3.1 Spatial and Temporal Complexity

Figure 1a-d shows the temporal evolution, measured in simulation time steps, of the slip rate along the fault surface during the earthquake cycle for four different cases with decreasing cohesion. As discussed earlier, cohesion contributed to bulk strength. The lower the bulk cohesion, the more prone to yielding the fault zone becomes. We observe that as bulk strength decreases, spatio-temporal complexity of the earthquake sequence emerges. This is evident in the transition from periodic events with slight variation in the nucleation characteristics, at $c = 35$ MPa, to intermittent earthquake with strong rupture segmentation and temporal clustering, for $c = 22$ MPa. Similar to observations in the antiplane deformations [38] plasticity accumulation around the rupture tip may result in the pinning of the rupture which in turn leads to local rupture arrest and spatial segmentation of coseismic slip. For all four cases shown here, the pattern of seismicity varies. We show that based on the choice of cohesion the ensuing seismic cycle can include partial ruptures, slow events, and intermittent episodes of earthquakes. This complexity is a direct consequence of the competition between on-fault and off-fault deformations.

In the case of $c = 35$ MPa, most of the events within the sequence are periodic and through-going with shifts in the nucleation site. In the cases of $c = 30$ MPa, and $c = 26$ MPa the sequence of events are quasi-complex. For the case of $c = 30$ MPa, seismicity converges to a sequence of doublets: a partial rupture followed by a through-going rupture and this combination keeps repeating. For the case of $c = 26$ MPa, the spatio-temporal complexity increases. However, the complex pattern appears to approximately repeat itself over longer time scales. The end member case with $c = 22$ MPa shows no distinguishable pattern and no diminished complexity with time.

To demonstrate the temporal complexity induced by plastic strain accumulation in Figure 1e we compare the time history of the peak slip rate for the two cases of $c = 35$ MPa and $c = 22$ MPa. We observe significant differences between the two cases in terms of the inter-event time, peak slip rates, and the emergence of foreshocks and aftershocks. Figure 1f focuses on the seismic activity leading up to a number of mainshocks (marked by the stars) in the case of $c = 22$ MPa. Here, we define the mainshock as an event with peak slip rate exceeding 0.1 m/s. We observe that the slip rate on the fault surface doesn't change gradually, but rather through a burst of microseismicity leading up to the mainshock. This temporal complexity results from plasticity accumulation and stress redistribution which controls the growth and arrest of these transients. Zoomed-in panels in Figure 1f expand on this observation and by focusing on the few seconds to minutes around the time of occurrence of the main shock. What appears as a single spike in Figure 1e on the scale of years is indeed a complex sequence of clustered seismic activity with intermittent episodes of earthquakes characterized by closely spaced bursts of accelerated motion associated with spontaneous nucleation and arrest of the rupture front multiple times.

To further quantify the effect of plastic strain accumulation on seismicity pattern, we analyze the variability in some of the statistical characteristics of the seismic sequence with variations in the bulk strength. For example, Figure 1g-j shows the distribution of recurrence interval for each of the four values of the cohesion parameter investigated here. We observe that the choice of bulk strength has significant implications on the clustering of seismicity. At higher cohesion, the events are periodic in time with uniform interevent time (year). As the yield stress decrease, we observe a shift in the recurrence interval toward interevent times that are orders of magnitude smaller. Eventually, the recurrence interval distribution as shown in Figure 1j transitions to an almost bimodal distribution with a heavy tail that spans time scales from seconds to days. This transition is characteristic of the emergence of seismic swarms.

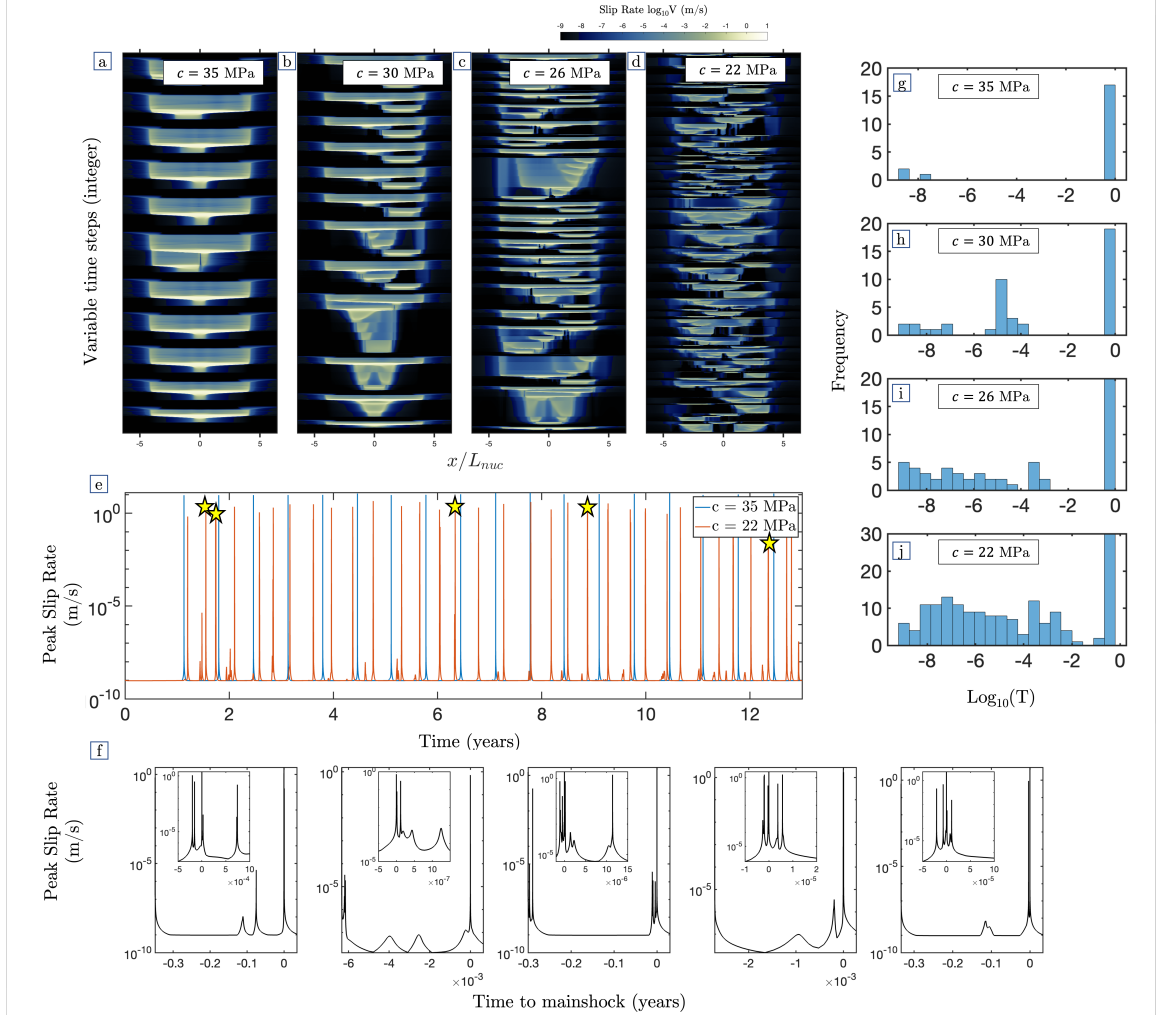


Figure 1: **Sequence of earthquakes and aseismic slip on a 2D in-plane rate-and-state fault.** (a-d) slip rate evolution with viscoplastic rheology illustrating increasing seismic complexity from periodic cycles to aperiodic sequence with segmented and partial ruptures as cohesion is reduced. (e) time history of the peak slip rate comparing $c = 35$ MPa with $c = 22$ MPa showing emergence of foreshocks and overall changes in recurrence pattern. (f) Time history panels showing foreshock patterns prior to mainshocks for several events highlighted by a yellow star in panel e. The zoomed in panels show individual event complexity. (g-j) Frequency distribution of interevent times highlighting the clustering behavior with reduction in bulk strength.

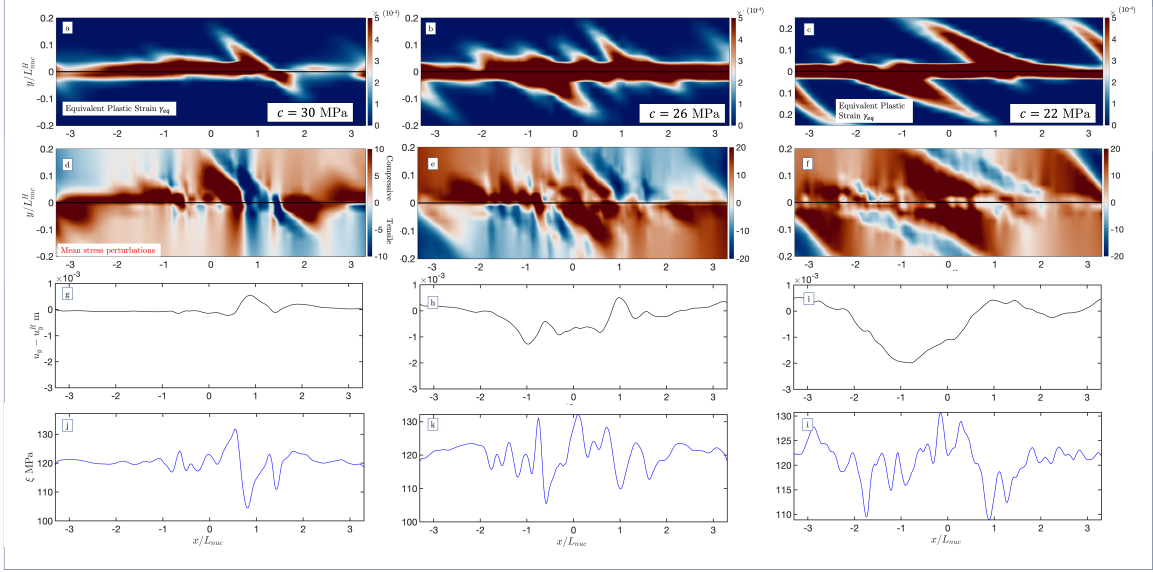


Figure 2: (a-c) The magnitude and extent of the equivalent plastic strain for three different cases of bulk cohesion $c = 30, 26,$ and 22 MPa at the end of the simulation showing varying patterns of accumulation based on the choice of bulk strength. (d-f) The mean stress distribution within the fault zone at the end of the earthquake cycle illustrating different evolution patterns based on the accumulated plasticity and seismic complexity. (g-i) The fault surface profile without the rotational component at the end of the cycle showing the emergence of short wave length fluctuations associated with fault zone structure evolution. (j-l) Associated changes in the normal stress on the fault demonstrating variations despite the planarity of the fault.

183 3.2 Evolution of Stress and Fault Structure

184 Simulations of single earthquakes demonstrate that the accumulation of plastic strain follows
 185 a specific pattern that is dictated by the choice of the angle of maximum compressive stress
 186 [44]. For the choices of $\Psi = 45^\circ$ the expected pattern of co-seismic plasticity is a fan-like
 187 distribution within the extensional quadrant of the bulk, defined by the sense of motion of
 188 the rupture front. In our analysis of sequences of earthquakes and aseismic slip, we instead
 189 observe a deviation from this expected pattern. Figure 2a-c show that at the end of the seismic
 190 sequence, the inelastic strain distribution is more broadly distributed in the near-fault region and
 191 accumulates on both sides of the fault. As discussed in [45], in addition, to rupture directivity,
 192 the accumulation of plastic strain in SEAS models is dictated by two other mechanisms. First,
 193 aseismic deformations induce changes in the mean stress field σ_m which influence the yield
 194 surface and create regions with lower mean stress that could favor plastic strain accumulation
 195 in subsequent dynamic ruptures. Also aseismic deformations may generate their own plasticity
 196 if the quasi-static stress concentration associated with the creeping fronts become large enough.
 197 Second, plastic strain accumulation causes residual mean stress changes. Specifically, mean stress
 198 becomes more compressive in regions where plasticity accumulates on the extensional side [44].
 199 However, changes in mean stress alters the yield strength which in turn impacts the potential for
 200 subsequent plastic strain accumulation. As a result, there is a correlation between plastic strain
 201 distribution and mean stress evolution. Furthermore, the mean stress field evolves, throughout
 202 the cycle, into a strongly heterogeneous distribution with alternating pockets of tensile and
 203 compressive perturbations relative to the initial mean stress value as shown in Figure 2d-f.

204 The magnitude, extent, and spatial distribution of the plastic strain depend on the fault zone
 205 strength as shown in 2a-c. As cohesion decreases, the width of the plastic zone increases and
 206 the magnitude of plastic strain becomes higher. This also correlates with larger variations in the
 207 mean stress that extend over larger distances away from the fault as shown in 2a-c. Importantly,

208 though, we observe that the width of the plastic zone in all cases is substantially smaller than the
 209 overall fault length and is on the order of a fraction of the nucleation zone size with a maximum
 210 extent of $0.2L_{nuc}$ for $c = 22$ MPa, which is approximately 3% of the total fault length. It is
 211 also important to note that the region with the most extensive plasticity accumulation is even
 212 smaller. This suggests that the implications of near fault plasticity on seismicity and stress
 213 evolution is significant despite the limited spatial extent and motivates further high resolution
 214 studies in the extreme vicinity of fault surfaces to characterize such inelastic processes.

215 Figure 2g-i illustrates the fault profile at the end of the simulation corresponding to different
 216 values of bulk cohesion. The fault profile is given by the magnitude of the transverse displace-
 217 ment u_y computed at the fault surface $y = 0$. For a homogeneous linear elastic medium, one
 218 expects a planar fault undergoing shear rupture to only rotate but remain primarily planar. The
 219 inelastic bulk rheology, however, leads to the emergence of partial ruptures due to the abrupt
 220 pinning of ruptures as well as stress heterogeneity. This results in the development of short
 221 wavelength undulations in the fault profile as shown in Figure 2g-i. To capture the variation
 222 in fault geometry in Figures 2g-i we only show the fault profile relative to overall fault rota-
 223 tion u_y^R . The fault rotation is computed by linearly fitting a displacement profile between the
 224 displacement at the right and the left ends of the VW patch of the fault. The magnitude and
 225 distribution of the undulations, referenced above, vary based on the choice of cohesion. Specifi-
 226 cally, we observe that for lower bulk strength, the undulations are more pronounced. They have
 227 larger amplitudes and vary over shorter wavelengths. On the other hand, for higher cohesion
 228 (e.g. $c = 30$ MPa), the fault profile, corrected for global rotation, remains almost flat. The
 229 undulations evolve throughout the cycle and contribute to the evolution of stress fields within
 230 in the near-fault region. The magnitude of these undulations is comparable to field observa-
 231 tions[46]. This suggests that bulk plasticity, and possibly other inelastic processes, may provide
 232 a self-roughening mechanism for faults, that has been largely understudied, even in the absence
 233 of initial roughness. Indeed, the role of pre-existing fault roughness has been previously high-
 234 lighted in the development of earthquake cycle and stress heterogeneity [47]. While we have not
 235 explored the role of the fault surface evolution on the slip dynamics explicitly, which requires
 236 solving the governing equations in the updated geometric configuration at each time step, the
 237 observed dynamic self-roughening mechanism is expected to contribute to the complexity of the
 238 seismic cycle, and dynamic rupture propagation [30, 34, 47, 48]. This observation suggests it
 239 might be important to consider the role of geometric nonlinearity (i.e adapting geometries) in
 240 models of sequences of earthquakes and aseismic slip.

241 Tied to the evolution of the fault surface profile, Figure 2j-l shows the end results of a
 242 corresponding evolution in the regularized normal stress ξ along the fault surface. The spatial
 243 variation in the normal stress is attributed to the combined effect of the emergence of short
 244 wavelength undulations and the nonuniform accumulation of plastic strain that cause different
 245 sides of the fault to deform differently in the fault normal direction. Although the fault surface is
 246 assumed to be initially planar, the normal stress heterogeneity emerge spontaneously and evolve
 247 throughout the sequence of events. However, the characteristics of this heterogeneity depend on
 248 the bulk strength and the cohesion value. Specifically, lower bulk strength enables shorter wave
 249 length variation in the spatial distribution of the normal stress. The peak value of the normal
 250 stress, however, is similar for all three cases.

251 To further understand the temporal evolution of fault zone plasticity based on the choice
 252 of bulk strength, Figure 3a-c illustrates the time history of the average plastic strain evolution
 253 in the near-fault region for three cases of decreasing cohesion $c = 30, 26,$ and 22 MPa. As
 254 expected, the magnitude of the average equivalent plastic strain increase with decreasing bulk
 255 strength. Similarly, we observe that the plasticity accumulated during the aseismic portion of
 256 the earthquake cycle also increases with decreasing bulk strength. Initially, during the early
 257 stages of the cycle, aseismic accumulation occurs rapidly, and then increases slowly throughout
 258 the cycle. Furthermore, we observe that the partitioning of plastic strain between the coseismic

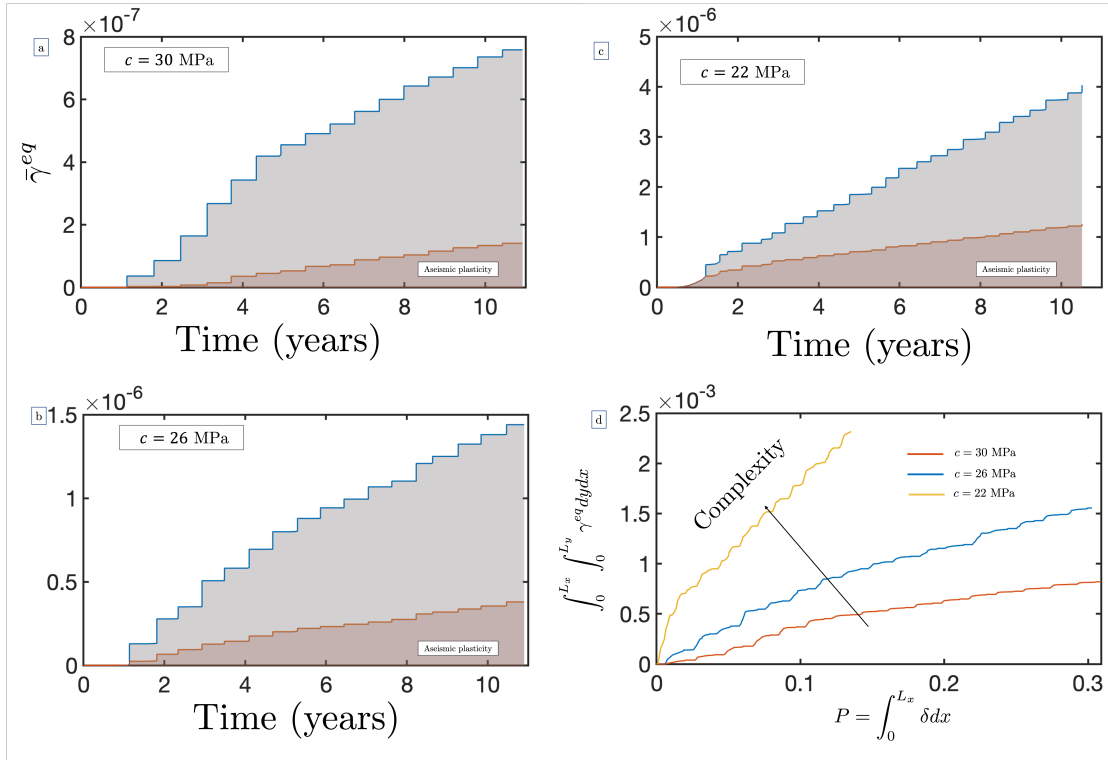


Figure 3: (a-b) Time history evolution of the average equivalent plastic strain within the off-fault bulk for three cases of different cohesion. Shading indicate partitioning between aseismic and coseismic plasticity. (d) The integrated equivalent plastic strain evolution with seismic potency indicating that complexity is associated with more bias toward off-fault deformations.

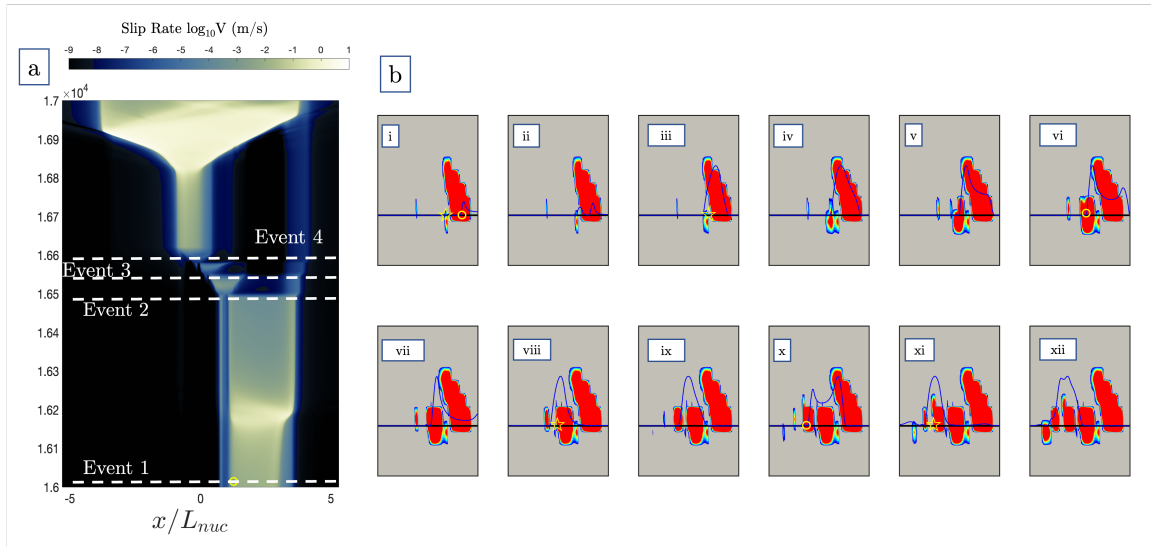


Figure 4: A specific snapshot for a cascading event presented for a case with cohesion $c = 30$ MPa. (a) The slip rate evolution for a viscoplastic 2-D fault illustrating cascading rupture propagation. (b) The partitioning between off-fault deformation and fault slip during this particular event sequence showing jerky rupture propagation in the form of individual events nucleation and arrest. The blue lines highlight the slip rate profile along the fault. The yellow circle indicate the location of rupture arrest, and the yellow star indicates the hypocenter of the renucleated rupture.

259 and aseismic phases also varies based on the choice of cohesion. As the cohesion decreases, a
 260 larger portion of overall plasticity accumulation is being accounted for aseismically. Specifically,
 261 by the end of the simulation, almost 19% of the total plastic strain is accumulated aseismically
 262 for $c = 30$ MPa. This fraction increased to 30% for $c = 22$ MPa. The increased role of aseismic
 263 plasticity partially explain the increased complexity in the seismicity and stress at lower bulk
 264 strength.

265 Finally, the partitioning of deformations between fault slip and off-fault plasticity plays a
 266 critical role in modulating the co-evolution of seismicity and fault zones. To highlight this, 3d
 267 shows the evolution of the integrated equivalent plastic strain within the near-fault region with
 268 fault slip expressed in terms of potency. There are two key observations: (1) the ratio between
 269 the integrated equivalent plastic strain and potency increases as the cohesion, and hence bulk
 270 strength, decreases, and (2) jumps associated with the increase in equivalent plastic strain are
 271 associated with minimal changes in potency. The first observation implies that complexity
 272 is proportional to the accumulation of plastic strain, with complexity being associated with
 273 more inelastic deformation delocalizing into the bulk. However, even for $c = 22$ MPa, the
 274 integrated equivalent plastic strain remain of the order of 1% of the seismic potency. The
 275 second observation suggests that there are periods during which it is more favorable for the
 276 deformation to be accommodated as bulk plasticity rather than fault slip. This, for example,
 277 may correspond to episodes of failed nucleation or arrested partial ruptures. In other words,
 278 these periods correspond to aseismic phases or episodes of transient slip deficit.

279 3.3 Cascading Earthquakes

280 Within our earthquake sequence with off-fault plasticity we observe the emergence of cascading
 281 earthquakes. These earthquakes just rupture, individually, a segment of the fault before
 282 arresting due to off-fault deformations. Nevertheless, due to a combination of (1) the favorable
 283 stress state and (2) the continuous creeping that concentrates the stress ahead of the pinned

284 rupture, subsequent earthquakes persistently nucleate along various segments of the fault in a
 285 brief timeframe, leading up to the eventual activation of the entire fault. Figure 4a shows the
 286 a cascading event sequence that occur for the case with cohesion $c = 30$ MPa. We observe
 287 the complexity of the earthquake sequence described above. Initially the rupture nucleates on
 288 the right side of the fault $x/L_{nuc} = 2.5$, the rupture propagate bilaterally prior to arresting
 289 due to inelastic strain accumulation. Eventually the stress concentration ahead of the pinned
 290 rupture tip is sufficient to trigger another rupture, which initiates ahead of the arrested event
 291 and rupture a new segment of the fault. This pattern keeps repeating with the triggering of
 292 event 3, and 4. Event 4 eventually rupture the whole seismogenic zone.

293 Figure 4c shows the rupture propagation as well as the pattern of plasticity accumulation
 294 within the bulk at different time steps within the cascading sequence of events. In panel (i-ii) We
 295 observe the onset of rupture arrest marked by the yellow circle accompanied by a substantial
 296 accumulation of off-fault plasticity. Within the same panel we highlight the location where
 297 the subsequent event will be triggered by a yellow star. The subsequent event is triggered
 298 ahead of the previously arrested panel as shown in panel (iii). In the intermediate panels (iii-v)
 299 the rupture proceeds to propagate prior to arresting in panel (vi) due to the accumulation of
 300 substantial inelastic strains. This pattern repeats again for the new ruptures that nucleates in
 301 panel (viii), and panel (xi).

302 This observed behavior is qualitatively similar to what has been observed in the quasi-static
 303 mode I fracture of elastic, perfectly plastic material in the plane strain configuration using the
 304 phase field approach[49]. Phase field models revealed that a plastic zone dulls the tip of a notch
 305 or crack, thereby impeding the initiation and spreading of the crack. When subjected to an
 306 adequate load, the crack initiates or unpins, but this occurs with a finite jump. As a result,
 307 the propagation is sporadic or abrupt, resulting in a rough surface. This jerky motion seems to
 308 persist for mode II dynamic fractures as observed here in our simulations suggesting a universal
 309 signature in elasto-plastic fracture phenomena.

310 4 Discussion

311 Our results indicate the accumulation of aseismic and coseismic off-fault deformation within the
 312 fault zone interact strongly with slip accumulation on the fault surface resulting in variations in
 313 the seismicity and stress patterns. In this work, we show that changing the bulk strength alters
 314 the earthquake sequence to produce complex slip patterns that depend on the extent of plastic
 315 strain accumulation. Based on the choice of bulk strength the fault surface exhibit a plethora of
 316 complex behavior such as partial ruptures, slow events, and intermittent episodes of earthquakes.
 317 The spatiotemporal complexity observed in our models is not tied to the particular choice of
 318 fault size[50], geometry[47] or heterogeneous distribution of frictional parameters. Rather, this
 319 complexity is attributed to the partitioning of deformation between fault slip and inelastic
 320 deformation in the bulk.

321 We have shown that plasticity accumulation produces persistent changes to the background
 322 stress field that influence the long term fault zone evolution and leads to emergence of regions
 323 of alternating compressive and tensile perturbations in the mean stress. Furthermore, our simu-
 324 lations highlight the role of bulk plasticity in the evolution of fault roughness and consequently
 325 short wavelength variations in the fault normal stress. These observations are consistent with
 326 recent experimental findings demonstrating that the sudden slip transition (in this particular
 327 case: the pinning of rupture tip) may produce substantial off-fault deformations and alter the
 328 fault surface in the fault normal direction [19].

329 Furthermore, we observe that the accumulation of off-fault inelastic deformations can lead to
 330 cascading sequence of events. This is due to accumulation of plastic zone which dulls the tip of
 331 the rupture front, thereby impeding the initiation and spreading of the rupture. Subjected to an
 332 sufficient load the rupture renucleate, however, with a finite jump. Consequently, the rupture

333 propagation becomes jerky, and within a short period of time (shorter than the recurrence
334 interval) several segments of the fault rupture independently. We note here that in the presence
335 of inelastic deformations we don't require any particular scaling of the fracture energy. Smaller
336 events are a direct consequence of more plastic dissipation and prior slip history, which eliminate
337 the need for fracture energy scaling (Gabriel et al., 2023) to achieve cascading events [51].
338 Furthermore, this study shows cascading events on a single fault that undergoes geometrical
339 and stress state evolution due to off-fault plasticity over seismic cycles. This observation of
340 cascading events is different from other cascading mechanisms involving elastic stress transfer
341 in fault segments or a network of faults [52–54].

342 We note that we have not studied very low cohesion values due to numerical instabilities
343 that emerge with the plasticity accumulation during the aseismic phases of the cycle prior to any
344 coseismic activity. However, recent work by Mia et al 2023, for antiplane deformations reveals
345 that as the rock strength is further reduced, the fault transitions into slow slip and seismicity
346 eventually shut off[39]. This limit remains to be studied in the in-plane case where aseismic
347 deformations can introduce mean stress perturbations and shift the yield envelope.

348 The main conclusions are summarized as follows:

- 349 1. Incorporating off-fault plasticity enable a transition from simple periodic through-going
350 events for higher bulk strength to chaotic sequences that exhibit temporal clustering and
351 spatial segmentation in the limit of lower bulk strength.
- 352 2. Accumulation of off-fault plasticity and emergence of partial ruptures lead to the evolution
353 of spatially heterogeneous normal stress field on the fault surface with short wavelength
354 variations, as well as, non-planar fault surface profile. For lower bulk strength, the fault
355 surface develop shorter wavelength undulations.
- 356 3. The overall plastic strain increases with decreasing bulk strength. The fraction of plastic
357 strain accumulated aseismically also increases with decreasing bulk strength.
- 358 4. The ratio between integrated plastic strain and potency increases with decreasing bulk
359 strength suggesting that a key mechanism for complex evolution of seismicity and stress
360 in fault zones lies in delocalizing of deformations. Lower bulk strength facilitates this
361 delocalization.
- 362 5. The extent of the fault zone that is plastically deforming remains very small compared to
363 the overall fault length. The ratio between the integrated plastic strain and potency is
364 also below 1% even for the lowest cohesion value considered in this study. Nonetheless,
365 the impact of bulk plasticity on seismicity and stresses is significant. This suggests the
366 need for further high resolution studies to characterize the complex near-fault response.
- 367 6. Off-fault plasticity present a possible mechanism for generating cascading earthquakes
368 without the need for fracture energy scaling. Cascading earthquakes and temporal cluster-
369 ing of earthquakes have been recently observed during the 2023 Herat earthquake sequence
370 [55]

371 **Acknowledgment**

372 M.A. would like to thank Ares Rosakis for insightful discussions. M.A. also acknowledges support
373 by the Caltech/MCE Big Ideas Fund (BIF), as well as the Caltech Terrestrial Hazard Obser-
374 vation and Reporting Center (THOR). The authors acknowledge support from the Southern
375 California Earthquake Center through a collaborative agreement between NSF. Grant Number:
376 EAR0529922 and USGS. Grant Number: 07HQAG0008 and the National Science Foundation
377 CAREER award No. 1753249 for modeling complex fault zone structures. This material is based
378 upon work supported by the Department of Energy under Award Number DE-FE0031685.

379 Data Availability

380 The authors accept AGU's data policy. Data generated from numerical simulations are uploaded
381 on CALTECH DATA repository and available online at <https://data.caltech.edu/records/nvvnq-qsg61>.
382

383 References

- 384 1. Chester, F. M., Evans, J. P. & Biegel, R. L. Internal structure and weakening mechanisms
385 of the San Andreas Fault. *Journal of Geophysical Research: Solid Earth* **98**, 771–786. ISSN:
386 01480227. <http://doi.wiley.com/10.1029/92JB01866> (Jan. 1993).
- 387 2. Mitchell, T. M. & Faulkner, D. R. The nature and origin of off-fault damage surrounding
388 strike-slip fault zones with a wide range of displacements: A field study from the Atacama
389 fault system, northern Chile. *Journal of Structural Geology* **31**, 802–816. ISSN: 01918141.
390 <http://dx.doi.org/10.1016/j.jsg.2009.05.002> (2009).
- 391 3. Huang, Y., Ampuero, J.-P. & Helmberger, D. V. Earthquake ruptures modulated by waves
392 in damaged fault zones. *Journal of Geophysical Research: Solid Earth* **119**, 3133–3154.
393 ISSN: 21699313. <http://doi.wiley.com/10.1002/2013JB010724> (Apr. 2014).
- 394 4. Huang, Y., Beroza, G. C. & Ellsworth, W. L. Stress drop estimates of potentially induced
395 earthquakes in the Guy-Greenbrier sequence. *Journal of Geophysical Research: Solid Earth*
396 **121**, 6597–6607. ISSN: 21699313. <http://doi.wiley.com/10.1002/2016JB013067> (Sept.
397 2016).
- 398 5. Barbot, S., Fialko, Y. & Sandwell, D. Effect of a compliant fault zone on the inferred
399 earthquake slip distribution. *Journal of Geophysical Research: Solid Earth* **113**, 1–10. ISSN:
400 21699356 (2008).
- 401 6. Lewis, M. A. & Ben-Zion, Y. Diversity of fault zone damage and trapping structures in
402 the Parkfield section of the San Andreas Fault from comprehensive analysis of near fault
403 seismograms. *Geophysical Journal International* **183**, 1579–1595. ISSN: 0956540X. [https:
404 //academic.oup.com/gji/article-lookup/doi/10.1111/j.1365-246X.2010.04816.x](https://academic.oup.com/gji/article-lookup/doi/10.1111/j.1365-246X.2010.04816.x)
405 (Dec. 2010).
- 406 7. Y.-G. Li & Leary, P. C. Fault zone trapped seismic waves. *Bulletin of the Seismological*
407 *Society of America* **80**, 1245–127 (1990).
- 408 8. Savage, H. M. & Brodsky, E. E. Collateral damage: Evolution with displacement of fracture
409 distribution and secondary fault strands in fault damage zones. *Journal of Geophysical*
410 *Research: Solid Earth* **116**. ISSN: 21699356 (Mar. 2011).
- 411 9. Biegel, R. L. & Sammis, C. G. *Relating Fault Mechanics to Fault Zone Structure* 2004.
- 412 10. Faulkner, D. R., Lewis, A. C. & Rutter, E. H. On the internal structure and mechanics
413 of large strike-slip fault zones: Field observations of the Carboneras fault in southeastern
414 Spain. *Tectonophysics* **367**, 235–251. ISSN: 00401951 (June 2003).
- 415 11. Weigandt, C., Griffith, W. & Rockwell, T. Role of confinement in coseismic pulveriza-
416 tion: Testing the rock record of rupture directivity on the San Jacinto fault, Southern
417 California. *Journal of Structural Geology* **177**, 104999. ISSN: 0191-8141. [https://www.
418 sciencedirect.com/science/article/pii/S019181412300216X](https://www.sciencedirect.com/science/article/pii/S019181412300216X) (2023).
- 419 12. Huang, Y., Ampuero, J.-P. & Helmberger, D. V. Earthquake ruptures modulated by waves
420 in damaged fault zones. *Journal of Geophysical Research: Solid Earth* **119**, 3133–3154.
421 eprint: <https://agupubs.onlinelibrary.wiley.com/doi/pdf/10.1002/2013JB010724>.
422 <https://agupubs.onlinelibrary.wiley.com/doi/abs/10.1002/2013JB010724> (2014).

- 423 13. Smith, Z. D. & Griffith, W. A. Evolution of Pulverized Fault Zone Rocks by Dynamic Ten-
424 sile Loading During Successive Earthquakes. *Geophysical Research Letters* **49**. e2022GL099971
425 2022GL099971, e2022GL099971. eprint: [https://agupubs.onlinelibrary.wiley.com/
426 doi/pdf/10.1029/2022GL099971](https://agupubs.onlinelibrary.wiley.com/doi/pdf/10.1029/2022GL099971). [https://agupubs.onlinelibrary.wiley.com/doi/
427 abs/10.1029/2022GL099971](https://agupubs.onlinelibrary.wiley.com/doi/abs/10.1029/2022GL099971) (2022).
- 428 14. Ben-Zion, Y. & Ampuero, J.-P. Seismic radiation from regions sustaining material damage.
429 *Geophysical Journal International* **178**, 1351–1356. ISSN: 0956-540X. eprint: [https://
430 academic.oup.com/gji/article-pdf/178/3/1351/5871906/178-3-1351.pdf](https://academic.oup.com/gji/article-pdf/178/3/1351/5871906/178-3-1351.pdf). [https://
431 //doi.org/10.1111/j.1365-246X.2009.04285.x](https://doi.org/10.1111/j.1365-246X.2009.04285.x) (Sept. 2009).
- 432 15. Ben-Zion, Y. & Lyakhovsky, V. Representation of seismic sources sustaining changes of
433 elastic moduli. *Geophysical Journal International* **217**, 135–139. ISSN: 0956-540X. eprint:
434 <https://academic.oup.com/gji/article-pdf/217/1/135/27662171/ggz018.pdf>.
435 <https://doi.org/10.1093/gji/ggz018> (Jan. 2019).
- 436 16. Lyakhovsky, V. & Ben-Zion, Y. Isotropic seismic radiation from rock damage and dila-
437 tancy. *Geophysical Journal International* **222**, 449–460. ISSN: 0956-540X. eprint: [https://
438 //academic.oup.com/gji/article-pdf/222/1/449/33181717/ggaa176.pdf](https://academic.oup.com/gji/article-pdf/222/1/449/33181717/ggaa176.pdf). [https://
439 //doi.org/10.1093/gji/ggaa176](https://doi.org/10.1093/gji/ggaa176) (Apr. 2020).
- 440 17. Kwiatek, G. & Ben-Zion, Y. Assessment of P and S wave energy radiated from very small
441 shear-tensile seismic events in a deep South African mine. *Journal of Geophysical Research:
442 Solid Earth* **118**, 3630–3641. eprint: [https://agupubs.onlinelibrary.wiley.com/doi/
443 pdf/10.1002/jgrb.50274](https://agupubs.onlinelibrary.wiley.com/doi/pdf/10.1002/jgrb.50274). [https://agupubs.onlinelibrary.wiley.com/doi/abs/10.
444 1002/jgrb.50274](https://agupubs.onlinelibrary.wiley.com/doi/abs/10.1002/jgrb.50274) (2013).
- 445 18. Cheng, Y., Wang, X., Zhan, Z. & Ben-Zion, Y. Isotropic Source Components of Events in
446 the 2019 Ridgecrest, California, Earthquake Sequence. *Geophysical Research Letters* **48**.
447 e2021GL094515 2021GL094515, e2021GL094515. eprint: [https://agupubs.onlinelibrary.
448 wiley.com/doi/pdf/10.1029/2021GL094515](https://agupubs.onlinelibrary.wiley.com/doi/pdf/10.1029/2021GL094515). [https://agupubs.onlinelibrary.
449 wiley.com/doi/abs/10.1029/2021GL094515](https://agupubs.onlinelibrary.wiley.com/doi/abs/10.1029/2021GL094515) (2021).
- 450 19. Ross, E. O., Reber, J. E. & Titus, S. J. Relating Slip Behavior to Off-Fault Deformation
451 Using Physical Models. *Geophysical Research Letters* **49**. ISSN: 0094-8276 (June 2022).
- 452 20. Ben-Zion, Y. & Sammis, C. G. Characterization of fault zones. *Pure and Applied Geophysics*
453 **160**, 677–715. ISSN: 00334553 (2003).
- 454 21. Abdelmeguid, M. & Elbanna, A. Modeling Sequences of Earthquakes and Aseismic Slip
455 (SEAS) in Elasto-Plastic Fault Zones With a Hybrid Finite Element Spectral Bound-
456 ary Integral Scheme. *Journal of Geophysical Research: Solid Earth* **127**. e2022JB024548
457 2022JB024548, e2022JB024548. eprint: [https://agupubs.onlinelibrary.wiley.com/
458 doi/pdf/10.1029/2022JB024548](https://agupubs.onlinelibrary.wiley.com/doi/pdf/10.1029/2022JB024548). [https://agupubs.onlinelibrary.wiley.com/doi/
459 abs/10.1029/2022JB024548](https://agupubs.onlinelibrary.wiley.com/doi/abs/10.1029/2022JB024548) (2022).
- 460 22. Rice, J. R., Sammis, C. G. & Parsons, R. Off-fault secondary failure induced by a dynamic
461 slip pulse. *Bulletin of the Seismological Society of America* **95**, 109–134. ISSN: 00371106
462 (Feb. 2005).
- 463 23. Mitchell, T. M. & Faulkner, D. R. Towards quantifying the matrix permeability of fault
464 damage zones in low porosity rocks. *Earth and Planetary Science Letters* **339-340**, 24–31.
465 ISSN: 0012821X (July 2012).
- 466 24. Childs, C. *et al.* A geometric model of fault zone and fault rock thickness variations. *Journal*
467 *of Structural Geology* **31**, 117–127. ISSN: 01918141 (Feb. 2009).

- 468 25. Heap, M. J., Faulkner, D. R., Meredith, P. G. & Vinciguerra, S. Elastic moduli evolution
469 and accompanying stress changes with increasing crack damage: Implications for stress
470 changes around fault zones and volcanoes during deformation. *Geophysical Journal Inter-*
471 *national* **183**, 225–236. ISSN: 0956540X (Oct. 2010).
- 472 26. Chester, J. S., Chester, F. M. & Kronenberg, A. K. Fracture surface energy of the Punch-
473 bowl fault, San Andreas system. *Nature* **437**, 133–136. ISSN: 0028-0836. <http://www.nature.com/articles/nature03942> (Sept. 2005).
- 475 27. Griffith, W. A., Nielsen, S., Di Toro, G. & Smith, S. A. Rough faults, distributed weak-
476 ening, and off-fault deformation. *Journal of Geophysical Research: Solid Earth* **115**. ISSN:
477 21699356 (Aug. 2010).
- 478 28. Mutlu, O. & Pollard, D. D. On the patterns of wing cracks along an outcrop scale flaw:
479 A numerical modeling approach using complementarity. *Journal of Geophysical Research:*
480 *Solid Earth* **113**. ISSN: 21699356 (June 2008).
- 481 29. Manighetti, I., King, G. & Sammis, C. G. The role of off-fault damage in the evolution of
482 normal faults. *Earth and Planetary Science Letters* **217**, 399–408. ISSN: 0012821X. <https://linkinghub.elsevier.com/retrieve/pii/S0012821X03006010> (Jan. 2004).
- 484 30. Tal, Y. & Faulkner, D. The Effect of Fault Roughness and Earthquake Ruptures on the
485 Evolution and Scaling of Fault Damage Zones. *Journal of Geophysical Research: Solid Earth*
486 **127**. ISSN: 2169-9313 (Jan. 2022).
- 487 31. Perrin, C., Manighetti, I., Ampuero, J. P., Cappa, F. & Gaudemer, Y. Location of largest
488 earthquake slip and fast rupture controlled by along-strike change in fault structural ma-
489 turity due to fault growth. *Journal of Geophysical Research: Solid Earth* **121**, 3666–3685.
490 ISSN: 21699356 (May 2016).
- 491 32. Faulkner, D. R., Mitchell, T. M., Jensen, E. & Cembrano, J. Scaling of fault damage zones
492 with displacement and the implications for fault growth processes. *Journal of Geophysical*
493 *Research: Solid Earth* **116**. ISSN: 21699356 (May 2011).
- 494 33. Anders, M. H. & Wiltschko, D. V. *Microfracturing, paleostress and the growth of faults*
495 tech. rep. 6 (1994), 795.
- 496 34. Dunham, E. M., Belanger, D., Cong, L. & Kozdon, J. E. Earthquake ruptures with strongly
497 rate-weakening friction and off-fault plasticity, part 1: Planar faults. *Bulletin of the Seis-*
498 *mological Society of America* **101**, 2296–2307. ISSN: 00371106 (2011).
- 499 35. Huang, Y. & Ampuero, J.-P. Pulse-like ruptures induced by low-velocity fault zones. *Jour-*
500 *nal of Geophysical Research* **116**, B12307. ISSN: 0148-0227. [http://doi.wiley.com/10.](http://doi.wiley.com/10.1029/2011JB008684)
501 [1029/2011JB008684](http://doi.wiley.com/10.1029/2011JB008684) (Dec. 2011).
- 502 36. Thakur, P., Huang, Y. & Kaneko, Y. Effects of Low-Velocity Fault Damage Zones on Long-
503 Term Earthquake Behaviors on Mature Strike-Slip Faults. *Journal of Geophysical Research:*
504 *Solid Earth* **125**, 1–20. ISSN: 21699356 (2020).
- 505 37. Erickson, B. A., Dunham, E. M. & Khosravifar, A. A finite difference method for off-fault
506 plasticity throughout the earthquake cycle. *Journal of the Mechanics and Physics of Solids*
507 **109**, 50–77. ISSN: 00225096. <http://dx.doi.org/10.1016/j.jmps.2017.08.002> (2017).
- 508 38. Mia, M. S., Abdelmeguid, M. & Elbanna, A. E. Spatio-Temporal Clustering of Seismicity
509 Enabled by Off-Fault Plasticity. *Geophysical Research Letters* **49**. ISSN: 19448007 (Apr.
510 2022).
- 511 39. Mia, M. S., Abdelmeguid, M. & Elbanna, A. E. The spectrum of fault slip in elastoplastic
512 fault zones. *Earth and Planetary Science Letters* **619**, 118310. ISSN: 0012-821X. <https://www.sciencedirect.com/science/article/pii/S0012821X23003230> (2023).
- 513

- 514 40. Cochard, A. & Rice, J. R. Fault rupture between dissimilar materials: Ill-posedness, reg-
515 ularization, and slip-pulse response. *Journal of Geophysical Research: Solid Earth* **105**,
516 25891–25907. ISSN: 01480227. <http://doi.wiley.com/10.1029/2000JB900230> (Nov.
517 2000).
- 518 41. Ranjith, K. & Rice, J. R. *Slip dynamics at an interface between dissimilar materials* tech.
519 rep. (2001), 341–361. www.elsevier.com/locate/jmps.
- 520 42. Tal, Y., Rubino, V., Rosakis, A. J. & Lapusta, N. Illuminating the physics of dynamic fric-
521 tion through laboratory earthquakes on thrust faults. *Proceedings of the National Academy*
522 *of Sciences* **117**, 21095–21100. ISSN: 0027-8424. [http://www.pnas.org/lookup/doi/10.](http://www.pnas.org/lookup/doi/10.1073/pnas.2004590117)
523 [1073/pnas.2004590117](http://www.pnas.org/lookup/doi/10.1073/pnas.2004590117) (Sept. 2020).
- 524 43. Abdelmeguid, M., Ma, X. & Elbanna, A. A Novel Hybrid Finite Element-Spectral Boundary
525 Integral Scheme for Modeling Earthquake Cycles: Application to Rate and State Faults
526 With Low-Velocity Zones. *Journal of Geophysical Research: Solid Earth* **124**, 12854–12881.
527 ISSN: 21699356 (Dec. 2019).
- 528 44. Templeton, E. L. & Rice, J. R. Off-fault plasticity and earthquake rupture dynamics: 1.
529 Dry materials or neglect of fluid pressure changes. *Journal of Geophysical Research: Solid*
530 *Earth* **113**, 1–19. ISSN: 21699356 (2008).
- 531 45. Abdelmeguid, M. & Elbanna, A. Modeling Sequences of Earthquakes and Aseismic Slip
532 (SEAS) in Elasto-plastic Fault Zones with A Hybrid Finite Element Spectral Boundary
533 Integral scheme. <https://doi.org/10.1002/essoar.10511050.2>.
- 534 46. Renard, F. & Candela, T. in *Fault Zone Dynamic Processes* 195–215 (American Geophys-
535 ical Union (AGU), 2017). ISBN: 9781119156895. eprint: [https://agupubs.onlinelibrary.](https://agupubs.onlinelibrary.wiley.com/doi/pdf/10.1002/9781119156895.ch10)
536 [wiley.com/doi/pdf/10.1002/9781119156895.ch10](https://agupubs.onlinelibrary.wiley.com/doi/pdf/10.1002/9781119156895.ch10). [https://agupubs.onlinelibrary.](https://agupubs.onlinelibrary.wiley.com/doi/abs/10.1002/9781119156895.ch10)
537 [wiley.com/doi/abs/10.1002/9781119156895.ch10](https://agupubs.onlinelibrary.wiley.com/doi/abs/10.1002/9781119156895.ch10).
- 538 47. Cattania, C. & Segall, P. Precursory Slow Slip and Foreshocks on Rough Faults. *Journal*
539 *of Geophysical Research: Solid Earth* **126**. ISSN: 21699356 (Apr. 2021).
- 540 48. Romanet, P. & Ozawa, S. Fully Dynamic Earthquake Cycle Simulations on a Nonplanar
541 Fault Using the Spectral Boundary Integral Element Method (sBIEM). *Bulletin of the*
542 *Seismological Society of America* **112**, 78–97. ISSN: 0037-1106. eprint: [https://pubs.](https://pubs.geoscienceworld.org/ssa/bssa/article-pdf/112/1/78/5518864/bssa-2021178.1.pdf)
543 [geoscienceworld.org/ssa/bssa/article-pdf/112/1/78/5518864/bssa-2021178.1.](https://pubs.geoscienceworld.org/ssa/bssa/article-pdf/112/1/78/5518864/bssa-2021178.1.pdf)
544 [pdf](https://pubs.geoscienceworld.org/ssa/bssa/article-pdf/112/1/78/5518864/bssa-2021178.1.pdf). <https://doi.org/10.1785/0120210178> (Oct. 2021).
- 545 49. Brach, S., Tanné, E., Bourdin, B. & Bhattacharya, K. Phase-field study of crack nucleation
546 and propagation in elastic–perfectly plastic bodies. *Computer Methods in Applied Mechan-*
547 *ics and Engineering* **353**, 44–65. ISSN: 0045-7825. [https://www.sciencedirect.com/](https://www.sciencedirect.com/science/article/pii/S0045782519302300)
548 [science/article/pii/S0045782519302300](https://www.sciencedirect.com/science/article/pii/S0045782519302300) (2019).
- 549 50. Barbot, S. Modulation of fault strength during the seismic cycle by grain-size evolution
550 around contact junctions. *Tectonophysics* **765**, 129–145. ISSN: 00401951. [https://doi.](https://doi.org/10.1016/j.tecto.2019.05.004)
551 [org/10.1016/j.tecto.2019.05.004](https://doi.org/10.1016/j.tecto.2019.05.004) (2019).
- 552 51. Gabriel, A.-A., Garagash, D. I., Palgunadi, K. H. & Mai, P. M. *Fault-size dependent fracture*
553 *energy explains multi-scale seismicity and cascading earthquakes* 2023. arXiv: 2307.15201
554 [physics.geo-ph].
- 555 52. Palgunadi, K. H., Gabriel, A.-A., Garagash, D. I., Ulrich, T. & Mai, P. M. *Rupture Dynam-*
556 *ics of Cascading Earthquakes in a Multiscale Fracture Network* 2023. arXiv: 2307.14229
557 [physics.geo-ph].
- 558 53. Im, K. & Avouac, J.-P. Cascading foreshocks, aftershocks and earthquake swarms in a
559 discrete fault network. *Geophysical Journal International* **235**, 831–852. ISSN: 0956-540X.
560 eprint: [https://academic.oup.com/gji/article-pdf/235/1/831/50959708/ggad278.](https://academic.oup.com/gji/article-pdf/235/1/831/50959708/ggad278.pdf)
561 [pdf](https://academic.oup.com/gji/article-pdf/235/1/831/50959708/ggad278.pdf). <https://doi.org/10.1093/gji/ggad278> (July 2023).

- 562 54. Ozawa, S. & Ando, R. Mainshock and Aftershock Sequence Simulation in Geometrically
563 Complex Fault Zones. *Journal of Geophysical Research: Solid Earth* **126**. e2020JB020865
564 2020JB020865, e2020JB020865. eprint: [https://agupubs.onlinelibrary.wiley.com/
565 doi/pdf/10.1029/2020JB020865](https://agupubs.onlinelibrary.wiley.com/doi/pdf/10.1029/2020JB020865). [https://agupubs.onlinelibrary.wiley.com/doi/
566 abs/10.1029/2020JB020865](https://agupubs.onlinelibrary.wiley.com/doi/abs/10.1029/2020JB020865) (2021).
- 567 55. US Geological Survey. *M 6.3 - 34 km NNW of Herāt, Afghanistan* [https://earthquake.
568 usgs.gov/earthquakes/eventpage/us60001fn5/executive](https://earthquake.usgs.gov/earthquakes/eventpage/us60001fn5/executive).

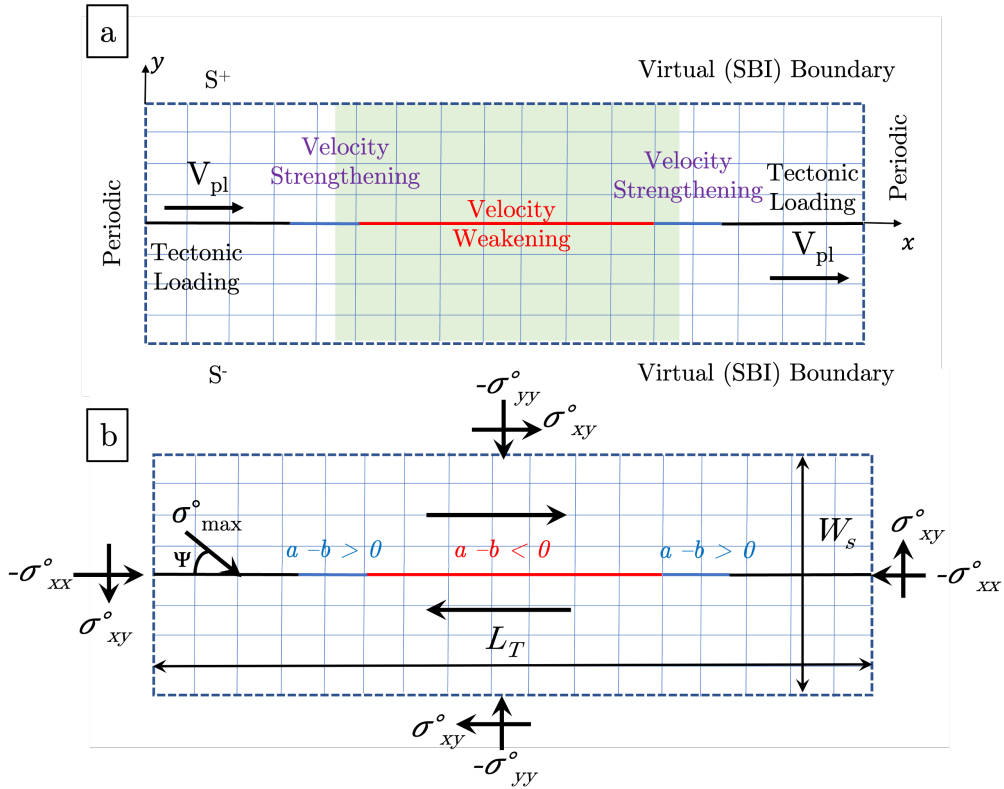


Figure A1: **Schematic of the model considered in this paper** (a) The computational setup for the hybrid FE-SBI scheme. A domain Ω adjacent to the fault surface is discretized using the finite element method. The spectral boundary integral method is utilized to model the external linearly elastic half spaces without explicit discretization. The response on the virtual boundaries parallel to the fault surface is expressed through an integral relation between the displacement and traction. Periodicity is imposed on the lateral boundaries of the domain. (b) The distribution of the fault frictional parameters and background tectonic stress field.

Table A1: Parameters description

Medium Parameter	Symbol	Value
Shear wave speed (km/s)	c_s	3.5
Pressure wave speed (km/s)	c_p	6.0
Density (kg/m ³)	ρ	2670.0
Length of the domain (m)	L_T	150
Distance between two virtual boundaries (m)	W_s	varies
Angle of Internal Friction	ϕ	31.6°
Cohesion MPa	c	varies
Angle of Maximum Compressive principal stress	Ψ	45°
Viscosity term (MPa-s)	η	0.32
Background Stress	Symbol	Value
Background Vertical Stress MPa	σ_{yy}	120
Background Horizontal Stress MPa	σ_{xx}	120
Background Shear Stress MPa	σ_{xy}	59.1
Fault Parameters	Symbol	Value
Static Coefficient of friction	f_o	0.6
Critical slip distance (μm)	L	50
Reference velocity (m/s)	V_o	10 ⁻⁶
Tectonic loading (m/s)	V_{pl}	10 ⁻⁹
Length of VW patch (m)	L_{VW}	50
Length of transition (m)	L_{VW-VS}	5
Length of the fault (m)	L_f	90
Evolution effect parameter	b	0.015
Steady state velocity dependence in VW patch	$(a_{VW} - b)$	-0.005
Steady state velocity dependence in VS patch	$(a_{VS} - b)$	0.015
Nucleation size (m)	L_{nuc}	6.96
Quasi-static process zone size (m)	L_b	1.2
Grid size (m)	Δx	0.1